Cretaceous Research 176 (2025) 106194

Contents lists available at ScienceDirect

Cretaceous Research

journal homepage: www.elsevier.com/locate/CretRes

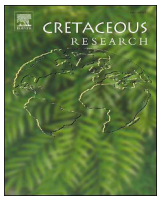

Integrated stratigraphy and paleoceanography across the Santonian/Campanian boundary in the Budva Zone (Dinarides), Montenegro

Anja Kocjančič [a,*], Maria Rose Petrizzo [b], Aleksander Horvat [a]

[a] Ivan Rakovec Institute of Palaeontology ZRC SAZU and Postgraduate School ZRC SAZU, Novi trg 2, SI-1000 Ljubljana, Slovenia
[b] Dipartimento di Scienze della Terra "A. Desio", Università degli Studi di Milano, via Mangiagalli 34, 20133 Milano, Italy

ARTICLE INFO

Article history:
Received 3 October 2024
Received in revised form
8 June 2025
Accepted in revised form 13 June 2025
Available online 26 June 2025

Keywords:
Upper Cretaceous
Planktonic foraminifera
Stratigraphy
Stable isotopes
Sr isotopes
Santonian/Campanian boundary

ABSTRACT

This paper examines the 42 m thick Upper Cretaceous sedimentary succession of the Čanj section in the Budva Zone (Dinarides), Montenegro, with a focus on planktonic foraminifera and geochemical characteristics across the Santonian/Campanian boundary. The section features well-preserved red pelagic Scaglia-type limestones with occasional chert intercalations, similar to the Cretaceous Oceanic Red Beds (CORBs) observed worldwide. An integrated stratigraphic analysis, including biostratigraphy and chemostratigraphy, was conducted to identify isotopic signals and planktonic foraminiferal species that characterize this Tethyan facies, and to locate the Santonian/Campanian boundary. The lithostratigraphic framework of the section includes distinct members (RM1, RM2, and RM3), along with a notable White Member (WM) containing black chert layers. Stable isotopes ($\delta^{13}C_{carb}$ and $\delta^{18}O_{carb}$) and elemental composition analyses on bulk carbonate samples reveal significant shifts in isotope ratios and element concentrations corresponding to lithologic transitions within the section. The occurrence of the planktonic foraminifera *Dicarinella asymetrica* in the WM marks an important biostratigraphic interval in the Santonian. The multiproxy approach revealed increased paleobioproductivity and a transgressive sea level phase in the WM during the Santonian in the western Tethys. Geochemical data suggest that the long-term sea-level rise was interrupted by smaller, short-term sea-level falls during the deposition of the studied pelagites. A comparative analysis with other Mediterranean CORBs and the Bottaccione section (Italy) highlights the regional significance of the Čanj sequence.
© 2025 The Authors. Published by Elsevier Ltd. This is an open access article under the CC BY license (http://creativecommons.org/licenses/by/4.0/).

1. Introduction

Upper Cretaceous deposits provide an extremely rich global database of past tectonic processes, climate variations such as changes from greenhouse to hothouse conditions, oceanic anoxic events, and sea-level changes, as well as information on paleoenvironments and changes in biota (Gale et al., 2020) using complementary stratigraphic methods and techniques such as biostratigraphy, magnetostratigraphy, and geochemistry. Despite all the progress made in this field of research, the Upper Cretaceous basin sequences in the Dinarides are still largely unexplored.

Our work in the Dinarides is focused on the Budva Zone in Montenegro (Fig. 1A, B), which is a belt of deep marine Mesozoic deposits about 10 km wide and about 100 km long (Goričan et al., 2022). Here we find remnants of the Budva Basin, which, due to its marginal position within the Dinaric orogen, was subject to continuous deep marine sedimentation from the Middle Triassic to the early Paleocene and thus provides an excellently preserved Upper Cretaceous stratigraphic record. The Upper Cretaceous basin sequence is characterized by Scaglia-type pelagic and hemipelagic limestones, and resedimented carbonates originating from the neighbouring High Karst Carbonate Platform.

Published research on the Budva Zone mostly describes the stratigraphy of the Upper Triassic to the Lower Cretaceous deposits (Cafiero and De Capoa Bonardi, 1980, 1981; Goričan, 1994; Črne et al., 2011), leaving the Upper Cretaceous interval almost unresolved. Previous paleontological studies in the Scaglia facies of the Budva Zone date back to the 1950s and were often part of a more general geological exploration of Montenegro (Nedela-Devide, 1957; Danilova, 1958).

In this paper we present an integrated stratigraphy of the Čanj section (Fig. 1B, C), the most distal Upper Cretaceous succession in the Budva Zone with an estimated palaeolatitude between 25.1°N and 28.3°N (van Hinsbergen et al., 2015). The section consists

* Corresponding author.
E-mail address: anja.kocjancic@zrc-sazu.si (A. Kocjančič).

https://doi.org/10.1016/j.cretres.2025.106194
0195-6671/© 2025 The Authors. Published by Elsevier Ltd. This is an open access article under the CC BY license (http://creativecommons.org/licenses/by/4.0/).

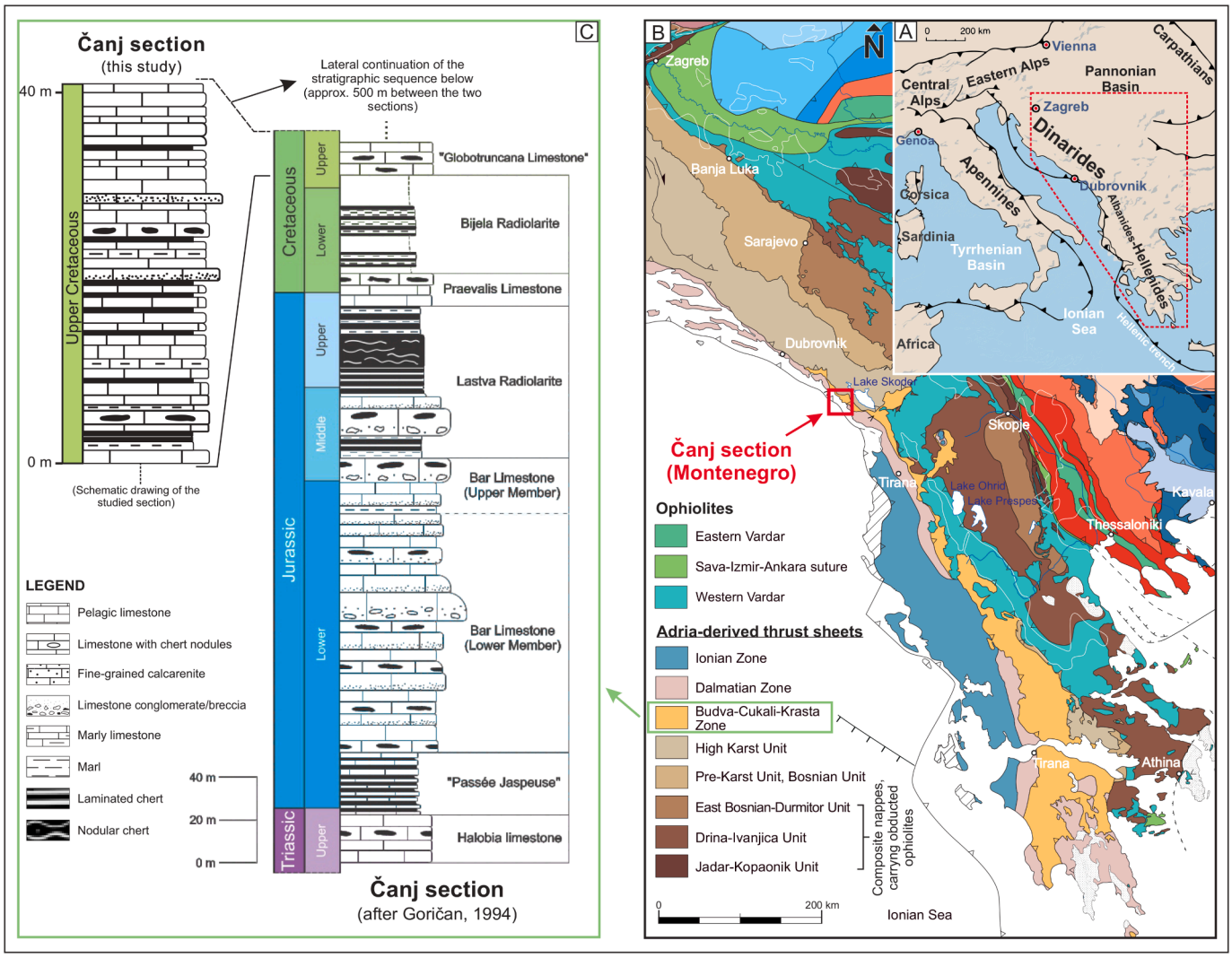

Fig. 1. Location and stratigraphy of the Čanj study section. (A) Current location of the Dinarides within the Alpine-Mediterranean chain with orogenic fronts and main basins (after Handy et al., 2015). The red square represents the location of B. (B) Geotectonic map of the Dinarides-Hellenides according to Schmid et al. (2008, 2020) with general location of the Čanj section within the Budva Zone. (C) Simplified column of lithostratigraphic units in the Čanj section with stratigraphic range of formations (modified after Goričan, 1994; Goričan et al., 2022) and the schematic lithological column of this study representing the Upper Cretaceous continuation of the section. The base of the Čanj section (this study) corresponds to the base of the *Globotruncana* Limestone of Goričan (1994).

almost exclusively of pelagic reddish-pink to brown Scaglia-type limestones. We present the lithological, sedimentological and micropaleontological composition of this pelagic sedimentary sequence and through stable isotopes and planktonic foraminiferal events identify the position of the Santonian/Campanian boundary.

In the literature similar Cretaceous fine-grained red pelagites are commonly referred to CORBs - Cretaceous Oceanic Red Beds (Scott et al., 2005; Wang et al., 2009) and have been described in many localities worldwide (Hu et al., 2005). However, CORBs have not yet been described in detail from the Budva Basin, making this work a new and original contribution to the understanding of CORB sedimentary sequences in the western Tethys. We briefly compare the red Čanj members with similar CORBs, particularly those from the Mediterranean region where Western Tethys remains are exposed (Fig. 2). The Čanj section also contains a distinct White Member (WM) (Fig. 3), composed of dark grey pelagic limestones interbedded with black chert layers, possibly indicating an enhanced influence of local processes that played a significant role in deposition. The sequence is also compared with well-established data from the Bottaccione section in Gubbio (Italy) a section that has been ratified as a Global boundary Stratotype Section and Point (GSSP) for the base of the Campanian Stage (Gale et al., 2023).

1.1. Geological setting of the studied section

The Čanj section is located near the beach of the small tourist town of Čanj on the coast of Montenegro. Structurally, the study area belongs to the Budva Zone in the External Dinarides (Fig. 1A, B). The Dinarides, together with the Albanides and Hellenides, form a single mountain chain with a common geodynamic history from the Triassic to the Early Cretaceous, consisting of rifting, obduction of ophiolites representing remnants of different Neotethys branches, erosion and formation of flysch and molasse basins (Stampfli and Borel, 2004; Schmid et al., 2008, 2020). Schmid et al. (2008, 2020 and references therein) have reviewed the regional framework of tectonic units from the Alps to western Turkey, and

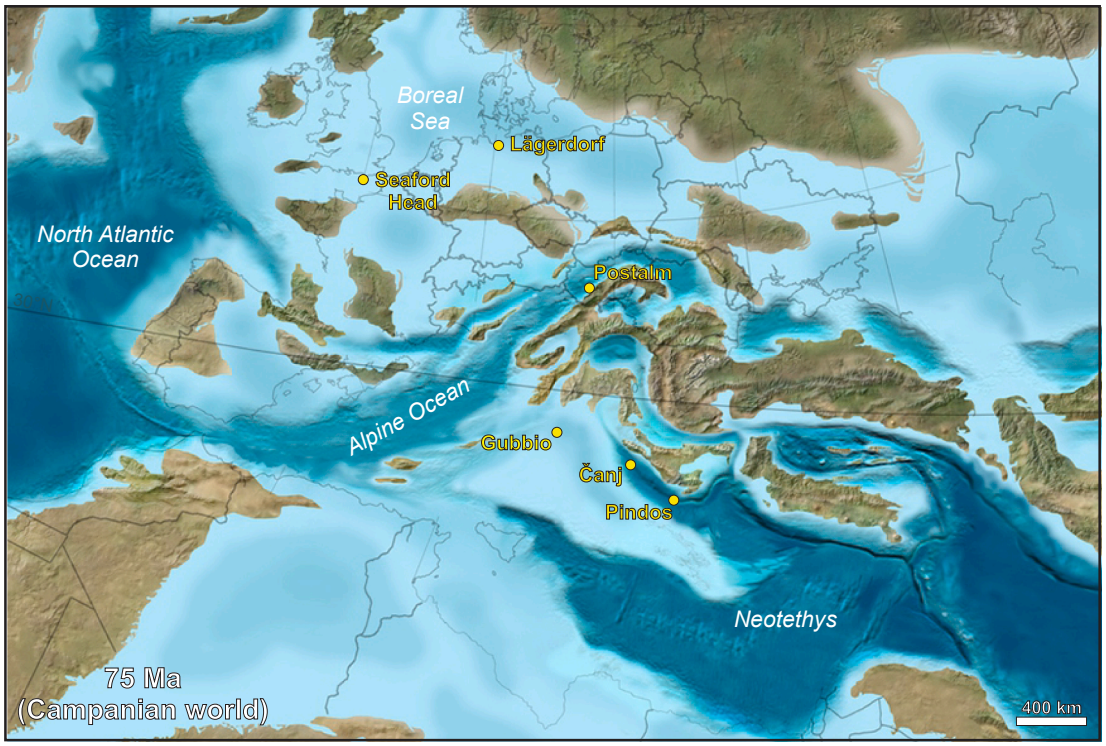

Fig. 2. Paleogeographic reconstruction of the Campanian (75 Ma). Map used with permission ©2012 Colorado Plateau Geosystems Inc. Names represent paleogeographic locations of Upper Cretaceous sections discussed in the text: Gubbio (Bottaccione section), Italy; Čanj, Montenegro; Pindos, Greece; Postalm, Austria; Seaford Head, UK; Lägerdorf, Germany.

Goričan et al. (2022) offered deeper insight into the evolution of Mesozoic basins of the southern Dinarides in Montenegro.

The structure of the Dinarides, which has been influenced by a prolonged extensional tectonic evolution and several phases of intense compressional tectonics and lateral shearing, consists of a series of SW-verging nappes derived from the eastern margin of the Adriatic microplate which was a relatively uniform shallow-water carbonate platform area until the Anisian. In the External Dinarides, where our section is located, the nappes consist of a thick sequence of Mesozoic carbonates of the Adriatic carbonate platform, interrupted along the southeastern margin by a Middle Triassic to Cretaceous rift trough, the Budva Zone (Goričan, 1994; 2022; Schmid et al., 2020). The Budva Zone itself consists of several complex thrust sheets which can be more generally divided into a lower and an upper tectonic subunit (Mirković et al., 1985). Based on previous stratigraphic studies, the upper subunit has thicker sequences of redeposited Jurassic-Cretaceous carbonates and is thus more proximal than the lower subunit (Goričan, 1994), in which the studied Čanj section is located.

The present-day Dinaric NW–SE striking tectonic units are in rough correspondence with Mesozoic paleogeography, and the SW–NE transect of these units in Montenegro and Serbia shows their excellently preserved stratigraphic successions (Schmid et al., 2020). Each tectonic unit corresponds to a different Mesozoic facies and paleotopography on the continental margin. Therefore, the arrangement of paleotopographic units in this transect from the outermost Dinarides towards the northeast is as follows (Fig. 1B): The Dalmatian Carbonate Platform (Dalmatian Zone), the Budva Basin (Budva-Cukali-Krasta Zone), which separates the High Karst Carbonate Platform (High Karst Zone) from the Dalmatian Zone, then the Bosnian Basin (Pre-Karst Unit and Bosnian Unit), the Durmitor High and the Lim Basin (East Bosnian-Durmitor Unit), the Drina-Ivanjica High (Drina-Ivanjica Unit) and the innermost composite nappe of the Dinarides, the Jadar-Kopaonik thrust sheet, which represents the outermost continental margin of the Adriatic plate (Schmid et al., 2020; Goričan et al., 2022).

The Budva Zone separates the lower Dalmatian Zone from the overlying High Karst Zone, which consists of Mesozoic platform carbonates. In the north it wedges out, while in the south it merges into the Krasta-Cukali Zone in Albania and further into the Pindos Zone in Greece (Schmid et al., 2020). The paleotopographic unit, the Budva Basin, was a V-shaped basin and a northern continuation of the Pindos Basin. In the Middle Triassic to Early Jurassic, the continental margin between the Pindos and Maliac Ocean (Stampfli and Borel, 2002) was subject to an extensional tectonic regime that produced a system of tectonic highs with carbonate platforms and troughs filled with pelagic sediments (horst-and-graben geometry). Due to its external position in the Dinaric orogen, the Budva Basin was an area of continuous pelagic sedimentation from the Middle Triassic to the Cretaceous. Through the Pindos Basin there was a very good connection to the very fertile surface waters of the central Neotethys (Goričan, 1994; Goričan et al., 2022). This led to high plankton productivity and the deposition of a high proportion of silica relative to carbonate, with radiolarian cherts as prominent pelagic sediment up to the lower Turonian (Goričan, 1994). Radiolarites in the Budva Basin characterized the Middle Triassic, the Hettangian–Sinemurian, the Aalenian–Tithonian and the Hauterivian–Barremian up to the lower Turonian (Goričan, 1994). Pelagic limestones predominate only in the Upper Triassic, Berriasian–Valanginian and upper Turonian–Maastrichtian, whereas calcareous turbidites from the adjacent High Karst Carbonate Platform are interbedded in all units (Goričan, 1994).

The Čanj section was studied in detail by Goričan (1994), who investigated the entire section, among other localities, describing a

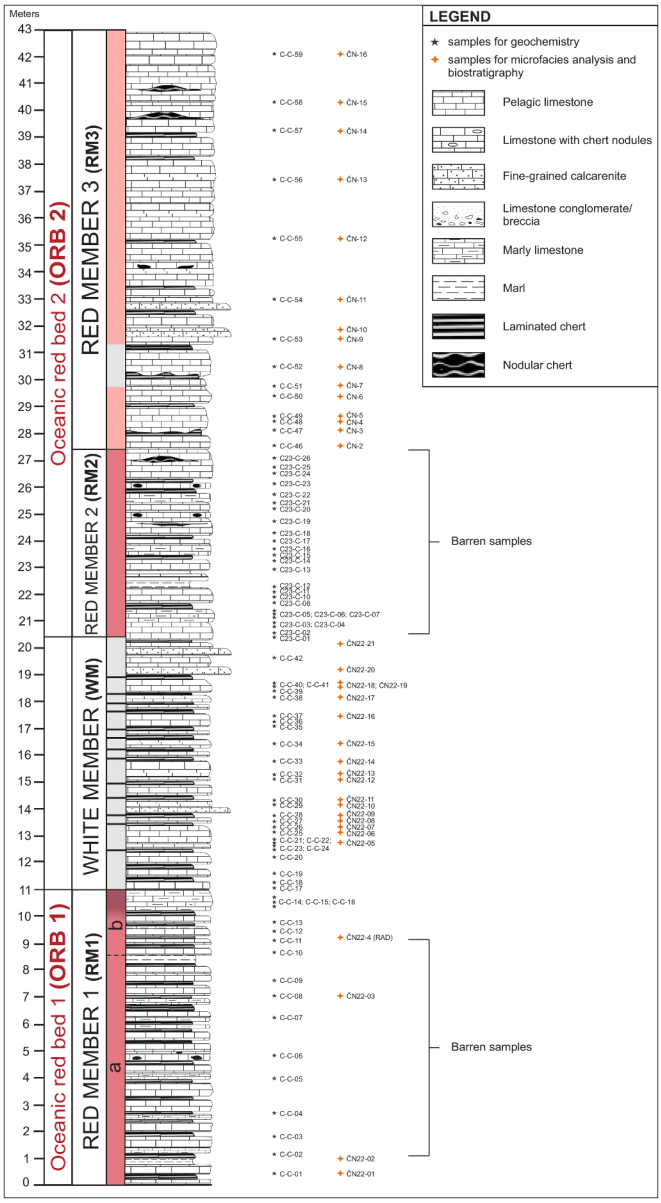

Fig. 3. Lithological column of the Čanj section. The thin black lines in the White Member represent the most evident intercalated black chert layers. Barren samples indicate sections lacking fossil data.

continuous deep-water succession from the Middle Jurassic to the Lower Cretaceous. The lower part of the section is rich in radiolarites, various types of pelagic limestones and intercalations of fine-grained resedimented carbonates, which are also mainly found in the lower parts of the section. The youngest age determined previously in Čanj was Turonian, based on radiolarian index fossils of the Bijela Radiolarites (Goričan, 1994; Goričan et al., 2022) (Fig. 1C). In this study, we focused on the upper part of the Čanj section, which comprises the pelagic and hemipelagic Upper Cretaceous red Scaglia-type sequences, generally described as *Globotruncana* Limestone (Nedela-Devide, 1957; Danilova, 1958).

2. Materials and methods

The investigated section is located in a small and abandoned quarry near a beach in the tourist town of Čanj in Montenegro (coordinates: N 42°09′50″, E 18°59′41″) (Fig. 1A, B). The 42 m of exposed Upper Cretaceous pelagic sediments are the subject of our research and were measured about 500 m lateral to the section investigated by Goričan (1994) (Figs. 1C, 3). The studied section comprises a stratigraphic interval of pink to red pelagic limestones with frequent chert intercalations and a distinct package of white pelagic limestones with dark chert layers in the middle of the section (Figs. 3, 4A). The studied interval overlies the last recorded, approximately 50 m thick package of the Bijela Radiolarite of Turonian age (Goričan, 1994) and corresponds to the base of the *Globotruncana* Limestone.

2.1. Sampling

A total of 86 samples of carbonate rocks were taken from the field. The sampling resolution varies between 10 cm and 2 m depending on the lithological composition. The sampling interval was more frequent around the foraminifera-bearing carbonate beds and for geochemical analysis, with samples collected at least 50 cm apart whenever possible (Fig. 3). All samples for biostratigraphic and geochemical analysis are listed in the Supplementary material S1 and stored in the Institute of Palaeontology ZRC SAZU in Ljubljana, Slovenia.

2.1.1. Planktonic foraminifera

For sedimentological and micropaleontological studies, 36 samples were prepared as standard thin sections. For the investigations of planktonic foraminifera, several thin sections of each sample were cut at different angles to the bedding in order to obtain thin sections for the identification of foraminifera in different orientations. The same samples were also prepared as washed residues with a 60–80 % acetic acid solution for different time intervals (from 4 to 24 h) until 150–200 g of the fragmented sample had disaggregated (methodology of Lirer, 2000; Falzoni et al., 2016). Due to the strong lithification of the limestone and the presence of common chert layers, many samples resulted incompletely disaggregated. Consequently, the planktonic foraminiferal specimens were mostly broken and corroded, making impossible the identification at species level. Only 4 washed samples were used for biostratigraphic analyses to complement the thin sections that were primarily used for the study.

The most abundant planktonic foraminifera taxa in thin sections were observed and photographed under the Olympus BX51 Polarizing Microscope. Genera and species were identified using illustrations and descriptions of taxa in the online taxonomic catalogue for Mesozoic planktonic foraminifera pforams@mikrotax portal (Huber et al., 2016). Various publications were also consulted to improve species identification in thin sections (Premoli Silva and Sliter, 1995; Premoli Silva and Verga, 2004; Petrizzo et al., 2011; Miniati et al., 2020). Biozonation and biostratigraphy follow Premoli Silva and Sliter (1995), Robaszynski and Caron (1995), Gale et al. (2020) and Petrizzo et al. (2025) for the western Tethys area. The full taxonomic list of planktonic foraminifera species is presented in Appendix 3.

Where the lithology permitted, samples were also taken for calcareous nannofossils. However, the slides prepared did not provide satisfactory results, as the nannoplankton specimens were poorly preserved or dissolved, and mostly absent.

2.2. Stable isotopes and geochemistry

Geochemical analyses were performed on 80 samples prepared (Fig. 3) for stable isotope analysis and determination of major and minor elements.

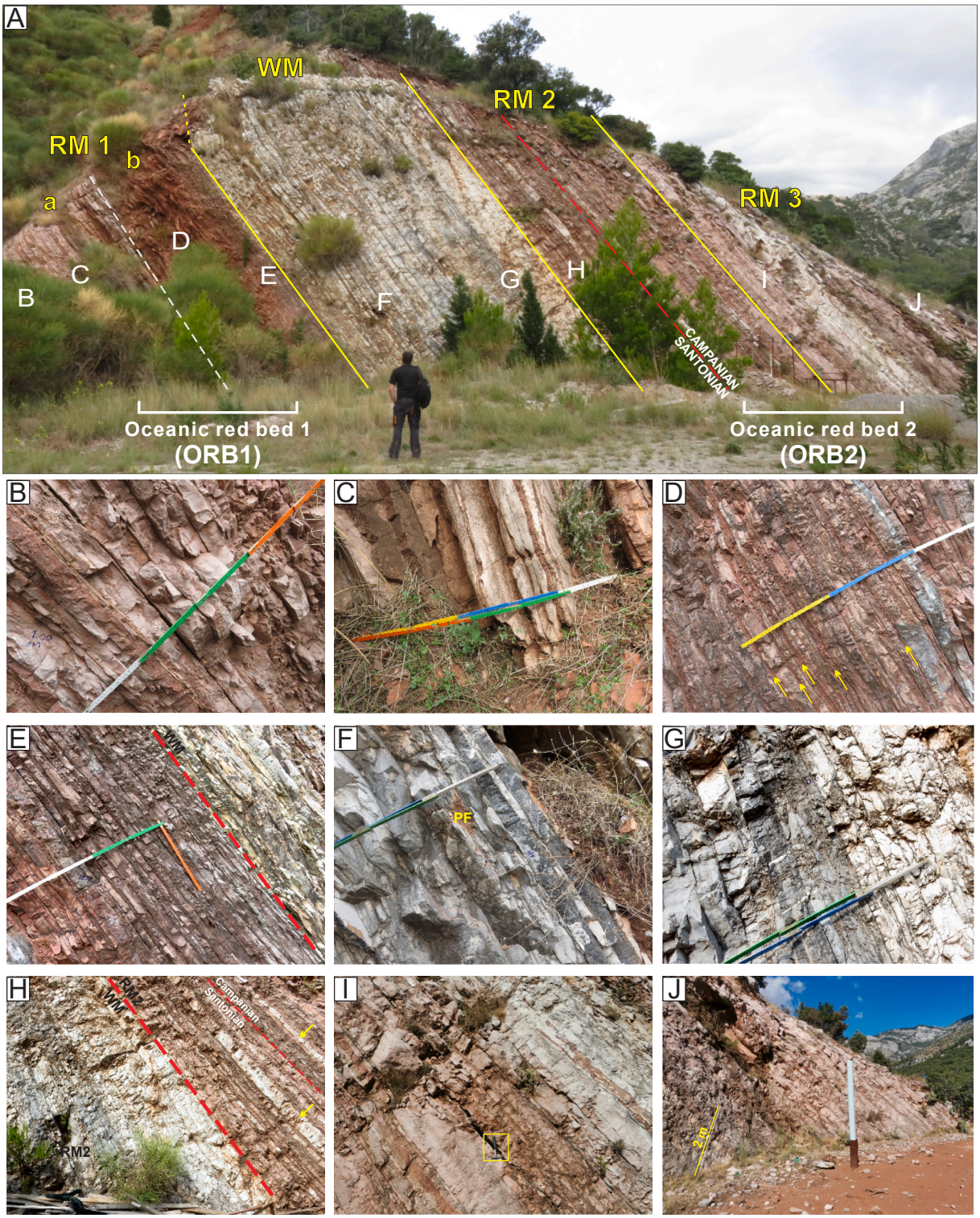

Fig. 4. (A) General field view of the Upper Cretaceous Čanj section with described/defined lithological members from Fig. 3. RM1, RM2 and RM3 are classified as Oceanic Red Beds (ORBs). Numbers in the middle of the section represent images of various transitions within and between members. (4B, 4C) Variations of light pink pelagic limestones with intercalations of laminated red cherts in the lower part of RM1-a. (4D) Dark red limestones with increased content of marl and marly limestones (yellow arrows) in between in the upper part of RM1-b. (4E) Transition between dark red limestone from image (4D) at the base through an 80 cm thick package of thin purple marly limestones towards the WM base (dotted red line). The $CaCO_3$ content in the purple limestones is lower with an average value of 72.4 %. (4F) Typical alternation between white limestones and dark grey to black chert layers in the WM, where the first planktonic foraminifera (PF) were recovered. (4G) Transition from light grey to white pelagic limestones in the WM. The light grey limestones often contain an increased number of planktonic foraminifera. (4H) General view of the transition between the WM and the RM2 (red dotted line). RM2 is barren of planktonic foraminifera and contains two thicker white limestone layers (yellow arrows), which are most likely recrystallized fine-grained calcarenites. In RM2, the Santonian/Campanian boundary was established based on carbon isotopes (see Fig. 7). (4I) Gradual transition between RM2 and RM3, containing a 1.5 m thick distinct package of white limestones (note the yellow square with a geologic hammer, 280 mm in length, serving as a scale). The chert content in this member is low compared to the other part of the Čanj section. Planktonic foraminifera are again present throughout RM3. (4J) View of the uppermost part of the Čanj section with light pink pelagic limestones of RM3. Notes on scale: in figure subsections B, C, D, E, F and G each fully extended colored line on the meter represents a length of 40 cm.

2.2.1. Stable carbon and oxygen isotope analysis

For the carbon ($\delta^{13}C_{carb}$) and oxygen ($\delta^{18}O_{carb}$) isotopes analysis, about 5 g of bulk carbonate samples were pulverized using a Dremel hand drill with diamond grit on the drill. The analysis of the pulverized samples was carried out at the Institute of Geological and Geochemical Research, Research Centre for Astronomy and Earth Sciences in Budapest, Hungary. The composition was determined using an automated carbonate preparation device (GASBENCH II) and a Thermo Finnigan delta plus XP continuous-flow mass spectrometer. Each sample was measured in duplicate and we report mean values in this article. The standard deviation values range between 0.02 and 0.07 for measured $\delta^{13}C_{carb}$ and 0.02 to 0.09 for $\delta^{18}O_{carb}$. Three laboratory standards were used to standardize the samples, which were calibrated with the reference materials NBS-18, NBS-19 and LSVEC (from the International Atomic Energy Agency). Based on these results, the accuracy and reproducibility of $\delta^{13}C_{carb}$ and $\delta^{18}O_{carb}$ values are better than ±0.1 ‰. The isotopic ratios of carbon and oxygen are reported as delta (δ) values in per mil (‰), relative to the V-PDB standard (Supplementary material S1).

2.2.2. Elemental analysis

Samples for bulk rock chemical analyses were prepared using the Fritsch Planetary Mono Mill Pulverisette 6, with approximately 20 g of each sample finely ground. Chemical analyses for the concentration of major elements (SiO_2, TiO_2, Al_2O_3, Fe_2O_3, MnO, MgO, CaO, Na_2O, K_2O and P_2O_5) and some minor elements (Ba, Be, Sr, Y, Sc, Zr and V) were performed by Activation Laboratories Ltd. in Ancaster, Ontario, Canada, using fusion ICP-AES (inductively coupled plasma-atomic emission spectroscopy). The rock samples were completely dissolved by lithium metaborate/tetraborate fusion and 5 % nitric acid digestion as described by Jarvis (2003). Four duplicates and ten standards (USGS and CANMET certified reference materials; Supplementary material S1) were used for quality control. Loss on ignition (LOI) was calculated based on the weight difference after ignition at 1000 °C. Precisions for major elements determined by ICP-AES were generally <3 % and <6 % for trace elements, with comparable accuracies for most determinations. The detection limits (DL) of elements and quality control are given in Supplementary material S1.

2.2.3. Strontium isotope analysis

The strontium isotope ratio was measured in 71 bulk rock samples from pelagic limestones. In almost all measured samples, the Sr content was well above 300 ppm (Supplementary material S1). The samples were first pulverized with a Dremel hand drill and stored in small vials. Analyses were carried out at the Institute of Geology, Mineralogy and Geophysics of the Ruhr-Universität Bochum, Germany. The samples were dissolved with different concentrations of HCl and HNO_3 in different runs, the element separation was carried out according to the standard procedures described by Mueller et al. (2020). The Sr fractions were loaded onto Re single filaments and the $^{87}Sr/^{86}Sr$ ratios were analysed using a Thermal Ionisation Mass Spectrometer (TIMS) TI-Box. Two international standards were used for long-term reproducibility: the NIST NBS 987 value of 0.710248 (McArthur et al., 2012) and the USGS EN-1 value of 0.709174 (McArthur et al., 2012). On various runs, an $^{87}Sr/^{86}Sr$ ratio of 0.709171 ± 0.000003 was determined for the USGS EN-1 Sr standard and raw ratios were adjusted accordingly to the NIST NBS 987 international standard of 0.710248 (McArthur et al., 2001). Some samples were corrected due to the presence of rubidium, which was still present during the measurements even though it was previously removed during the filament heating process (Appendix 1). The analytical errors of the $^{87}Sr/^{86}Sr$ ratios are reported as ±2 SE.

3. Results

3.1. Lithostratigraphic description of the section

The studied interval of the Čanj section overlies the Bijela Radiolarite, whose contact with the limestones is not exposed (Fig. 4; RM1-a). The section was subdivided into individual members based on lithological features such as color and composition. The sequence is continuous and shows no significant tectonic or depositional disturbances.

The section begins with the lowermost dark Red Member 1 (RM1), which is subdivided into lower RM1-a and upper RM1-b due to different lithological characteristics and geochemical composition. RM1 with a bed thickness of 11 m consists of light pink (in the lower RM1-a part) micritic limestones with an average thickness of 10 cm. The silica content constitutes approximately 30 % of the entire package. This is expressed as dark red cherty limestones, in which laminated (up to 5 cm) cherts without radiolarians often alternate. Replacement chert nodules are also present. The marl content increased only in the lower and upper parts (RM1-b) of this member (Figs. 3, 4B, 4D) where thin marl layers and marly limestone with an average thickness of 5 cm are common. RM1 ends with an 80 cm thick package of thin purple-red marly limestones interbedded with layers of laminated chert (Fig. 4A).

RM1-b is overlain by the White Member (WM), which is white to light gray in color (Fig. 4A). The contact between the two units is sharp, and the color change is highly pronounced. WM is 9.5 m thick and consists of white to light gray micritic limestones between 10 and 15 cm thick. Between these limestones are horizons of dark gray to black chert layers up to 10 cm thick. The micritic limestones are weakly laminated and sometimes contain horizons of calcisiltite. This WM member, in addition to a clear change in color, contains the first planktonic foraminifera above the first black chert layer between 12.5 and 13.5 m of the section. Above their lowest occurrence, the planktonic foraminifera are present throughout the entire WM member. The upper part of WM is characterized by two fine-grained calcarenite beds, each up to 10 cm thick. These are the only recognizable fine-grained resedimented carbonates in the studied section that remained unsilicified or un-recrystallized.

The WM is followed by a dark Red Member 2 (RM2), which is approximately 7 m thick. RM2 comprises dark red to brown-red micritic limestones interbedded with red chert layers and marls, mostly 1–3 cm thick (Fig. 4A). Dark red to brown marly limestones with a thickness of 1–5 cm are also common. The thickness of the micritic limestone beds is similar to that of RM1 (up to 10 cm, rarely 20 cm), with the exception of two thicker beds of white limestone, 35 and 12 cm thick respectively. The micritic limestones are often partially or completely silicified, chert lenses are abundant and unevenly distributed throughout the member. Red chert layers reach a thickness of up to 25 cm. There is no evidence of microfossils (calcareous nannoplankton or planktonic foraminifera) in the member, not even radiolarians in chert layers. The layers become thicker and the color changes to light pink towards the top of the interval. The transition between RM2 and the overlying RM3 member is gradual.

The uppermost member in the Čanj section is Red Member 3 (RM3) with an approximate thickness of 15.5 m. The beds in this member are pink to light red, interrupted by an approximately 1.5 m thick package of white-gray to light ochre micritic limestones (Fig. 4A). The thickness of the limestone beds varies between 15 cm and 70 cm, while red nodular chert is rare and occurs mainly in the lower part of the member. Red chert layers are rare compared to the other parts of the section and reach a thickness of

about 15 cm, thinning laterally or disappearing completely. Between 33 and 34 m height, the limestones are interbedded with two pink or light gray, silicified, fine-to medium-grained calcarenite layers with pronounced red grains that represent older resedimented lithologies. The thickness of these two resedimented layers is 17 cm and 4 cm respectively. Micropaleontological studies of this member revealed a continuous occurrence of planktonic foraminifera from the lowest to the uppermost part, including the 1.5 m thick package of white-grey limestone in between.

3.2. Limestone microfacies

The pelagic limestones are generally well cemented and mostly structureless mudstones (Fig. 5). Grains of small size (less than 100 μm) make up only 5–10 % of the matrix. Sporadically, (in the white and also in the pink limestone) thin, darker layers consisting of calcisiltite with indistinct grains may be observed. Individual sections of the white limestone (WM) contain calcite laminae or lenses a few millimeters thick, which are visible under the microscope as concentrations of planktonic foraminiferal tests (Fig. 5F). The tests are barely identifiable due to strong recrystallization, but a residue of organic material can often be seen in their cavities (Fig. 5G, H). In WM and RM3, the microfacies grades to planktonic foraminiferal wackestone and packstone. The foraminifera tests are generally filled with calcite cement and distributed within the matrix, but there are also distinct horizons or belts of foraminifera, possibly indicating periods of increased current deposition (fine-grained turbidites or contourites). In addition to foraminifera, inoceramid prisms are common in these horizons.

The calcarenite facies in sample ČN22-20 (WM) consists of fine-grained peloidal intraclastic grainstone. The microfacies is well sorted and has no distinct structures. The grain composition consists of micritic intraclasts, peloids, rare small benthic foraminifera (Fig. 5I) and poorly recognizable bioclastic fragments due to recrystallization of the matrix. In sample ČN10 sample (RM3), the calcarenite facies is a bioclastic planktonic foraminiferal grainstone. This microfacies is rich in planktonic foraminifera tests that are strongly recrystallized. Other bioclasts in this microfacies are rare fragments of echinoderms (echinoderm plates and spines) and small benthic foraminifera. Small red intraclasts representing grains of background micritic limestones also occur. In general, bioclastic fragments are poorly recognizable due to strong recrystallization and selective silicification. Small patches of micritic matrix are only sporadically preserved.

Another facies that is very rare and only occurs in the lowest part of the section (RM1) consists of radiolarian wackestone (Fig. 5E). Two horizons (at 9.5 and 12.75 m) can be observed in this microfacies, the first contains radiolarians in a carbonate matrix, the second has some sponge spicules in addition to radiolarians. Due to the strong recrystallization, the radiolarians could not be extracted using various preparation methods.

Almost all micritic thin sections contain calcite veins running in different directions. Silicification (Fig. 5J, K) is mainly observed in the fine-grained calcarenites, especially in the foraminifera grainstone, where it is bound to areas between foraminiferal tests and selectively to certain bioclasts. Microstylolites are common in mudstones and are found parallel to bedding.

3.3. Foraminiferal biostratigraphy

The study of planktonic foraminifera was mainly based on thin sections, in which the specimens can be easily identified. In the washed samples, the state of preservation of the tests is poor, with a high percentage of broken tests due to the processing of the rock samples. Planktonic foraminifera are abundant in mudstones of members WM and RM3, where they are generally diverse. The assemblage is typical of a tropical Tethyan realm, represented by the following morphological groups (Table 1; Appendix 3): biserial (*Planoheterohelix*, *Pseudotextularia*, *Laeviheterohelix, Pseudoguembelina*) and planispiral (*Planohedbergella*, *Laeviella* - previously classified within the genus *Globigerinelloides*; see Huber et al., 2020) taxa, low-trochospiral morphotypes (*Muricohedbergella*), higher-trochospiral forms with globular chambers (*Archaeoglobigerina*), multiserial forms (*Ventilabrella*), as well as abundant single-keeled (*Globotruncanita*) and double-keeled (*Dicarinella, Marginotruncana, Contusotruncana, Globotruncana*) taxa. The marker species and the most common taxa are illustrated in Fig. 6.

The lowermost part of the section (member RM1) comprises a 12.75 m thick barren interval above the Bijela Radiolarite and is characterized by the complete absence of foraminifera and apparently other organisms (Fig. 3). Planktonic foraminifera are first observed at 13.26 m above member RM1 in the WM and are quite abundant upward to the top of the member (at 21.10 m). In this stratigraphic interval (Table 1), the foraminifera are highly diverse, with *Marginotruncana* together with *Globotruncana* being the most abundant group of keeled foraminifera. Dicarinellids are common but are difficult to identify to species level due to the frequently broken tests. Small biserial forms, globigeriniform and planispiral taxa are constant, especially *Planohedbergella*, *Pseudoguembelina*, *Planoheterohelix* and *Laeviella*, although some of them are hardly recognizable at species level in thin section.

Following the section upward (Fig. 3; Table 1), the succession exhibits another barren interval represented by member RM2 (at 20.5 m). Above this gap planktonic foraminifera reappear with the marginotruncanids disappearing in the lower part of RM3 after 29.46 m. Globotruncanids increase in abundance and become the most common foraminifera among the deep-dwelling forms. *Globotruncanita elevata*, *Globotruncana linneiana* and *Globotruncana neotricarinata* are present throughout the entire section with the exception of RM2. This also applies to *Globotruncanita stuartiformis*, which appears more abundant only after RM2 with the decline in abundance of *G. elevata* (Table 1). Biserial forms are less diverse.

According to foraminiferal data the lower stratigraphic interval from 13.26 m to 18.7 m is assigned to the *Dicarinella asymetrica* Total Range Zone (Figs. 6, 7; Table 1). Despite its discontinuous occurrence in the section, the highest occurrence (HO) of the biostratigraphic marker *D. asymetrica* can be confidently placed at 18.7 m. The overlying interval, which spans from 18.7 m to 42.14 m is assigned to the *G. elevata* Interval Zone. This biostratigraphic interval of RM2 is barren of planktonic foraminifera for about 7 m (Fig. 7; Table 1). Some species of globotruncanids reappear above this second barren interval, including the marker species of the *G. elevata* Interval Zone, while others disappear completely (Fig. 7; Table 1).

The stratigraphic intervals above also contain secondary planktonic foraminiferal bioevents with their lowest (LO) and highest (HO) occurrence. In the *D. asymetrica* Zone the dicarinellids are present but difficult to determine at species level in thin sections. They are mainly represented by *D. asymetrica* and *Dicarinella concavata*. The secondary bioevents are listed in stratigraphic order (Fig. 7; Table 1): (1) LO of *G. neotricarinata* and *G. elevata* at 13.26 m; (2) HO of *D. concavata* at 13.41 m; (3) HO of *Marginotruncana tarfayaensis* at 16.5 m; (4) HO of *Marginotruncana sinuosa* at 18.7 m; (5) HO of *Marginotruncana pseudomarginata* at 20.1 m. Secondary foraminiferal events in the *G. elevata* Interval Zone include the: (1) HO of *Marginotruncana coronata* at 29.46 m; (2) LOs of

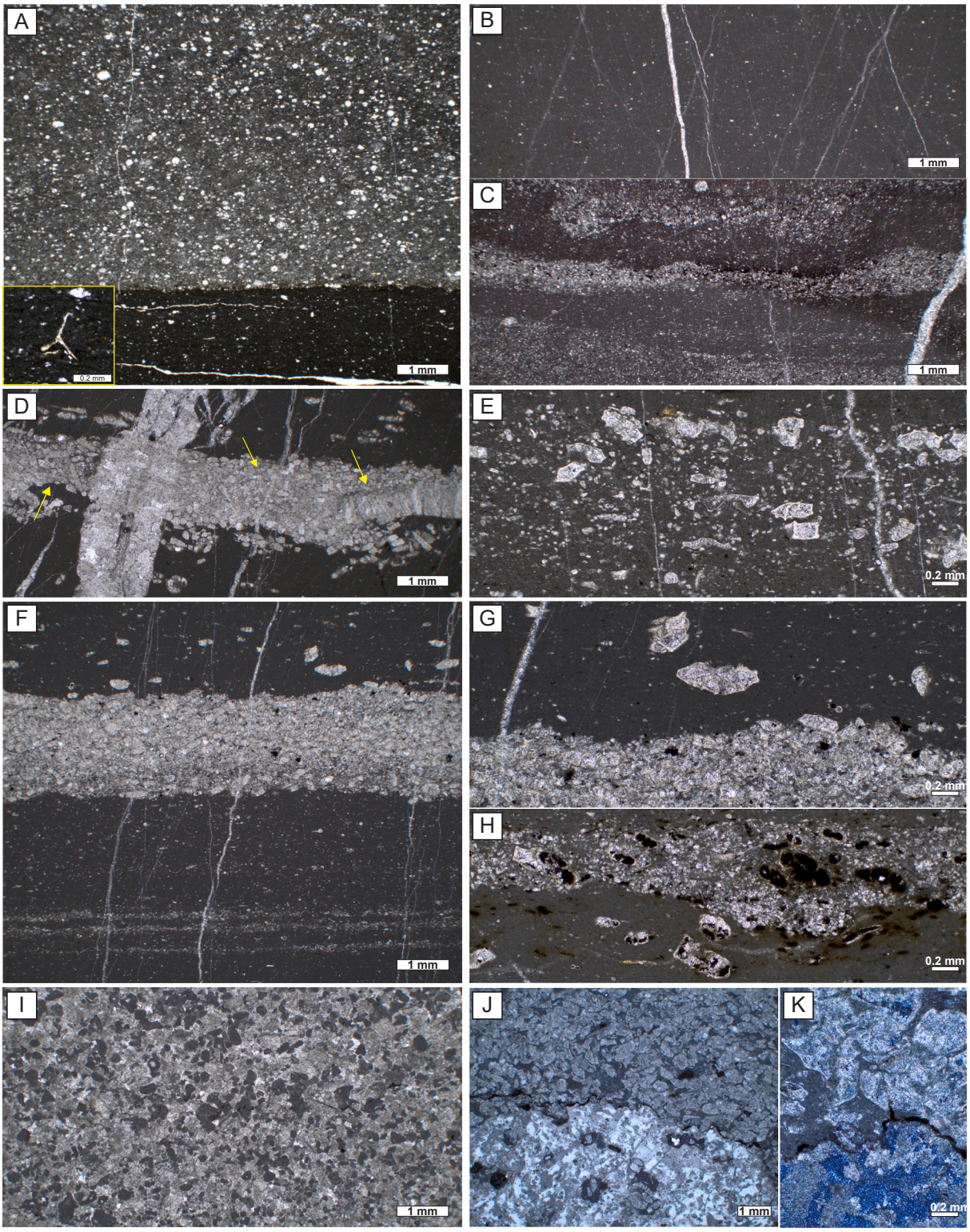

Fig. 5. Pelagic limestone microfacies of the Čanj section. (A) Radiolarian wackestone with a close-up of a sponge spicule present only in the lower, darker horizon (sample ČN22-5). (B) Typical microfacies of pelagic limestones - mudstone - with (C) fine-grained calciturbidite laminas (sample ČN22-6). (D) Accumulation of inoceramid fragments (yellow arrows) with cross cutting calcite veins (sample ČN22-8). (E) Foraminifera wackestone with indistinct fine grains. Based on a few well-preserved test sections, the foraminifera mostly belong to the genera *Marginotruncana* and *Dicarinella* (sample ČN22-17). (F) Horizon of accumulated planktonic foraminifera, possibly fine-grained turbidites or contourites, from the WM with a close-up of the foraminiferal tests and opaque grains in image (G) (sample ČN22-16). The picture is taken under parallel polars. (H) Foraminifera accumulation from the WM with opaque residues/fillings in the chambers (sample ČN22-15). (I) Well-sorted, fine-grained peloidal intraclastic grainstone (sample ČN22-20). (J, K) Foraminiferal packstone with partially silicified matrix and foraminifera tests: J under parallel polars, K a magnification image J under crossed polars (sample ČN-10).

Table 1
Stratigraphic distribution of planktonic foraminifera species in the Čanj section. LO = Lowest Occurrence, HO = Highest Occurrence.

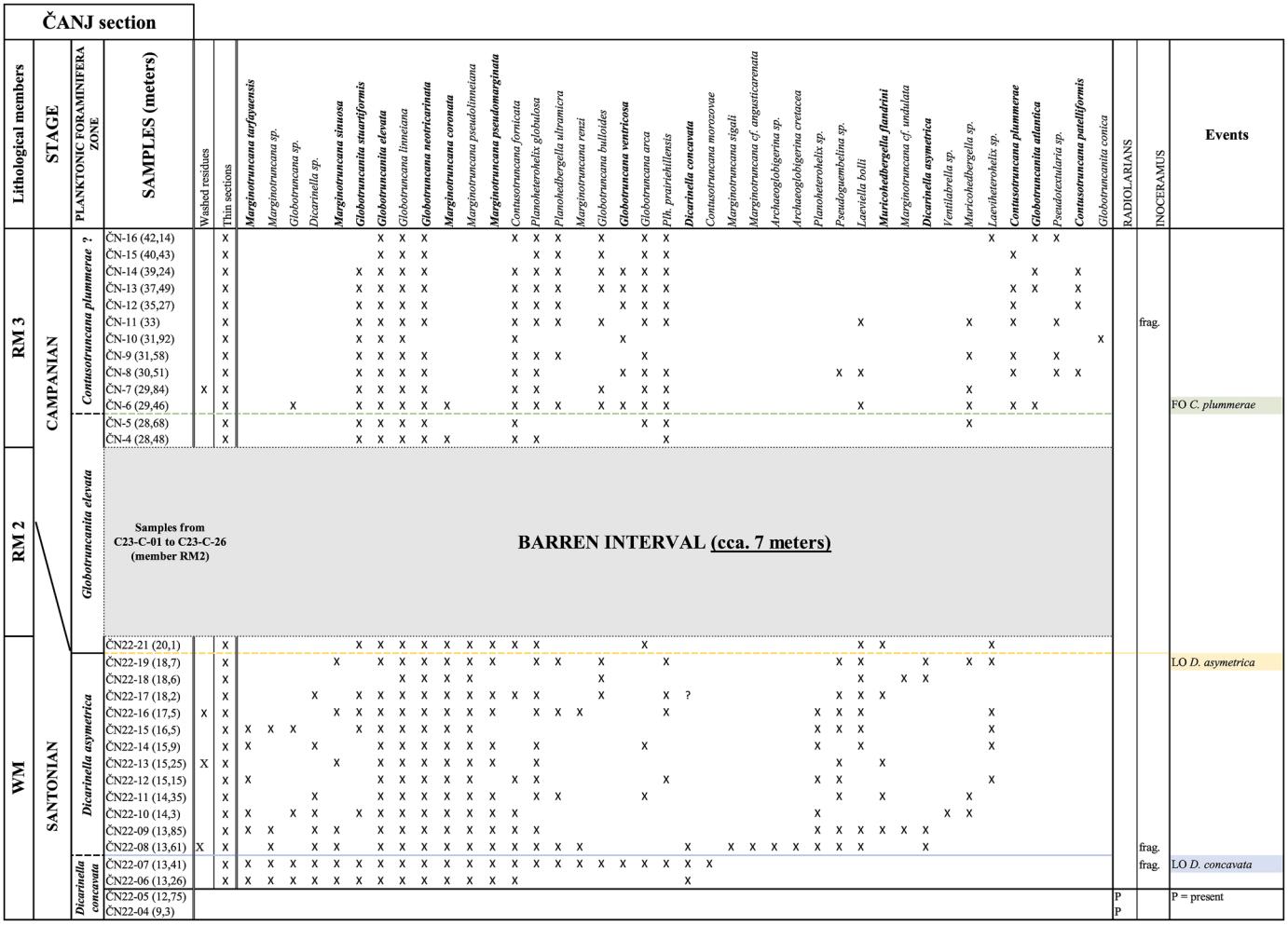

Globotruncana ventricosa and *Contusotruncana plummerae* at 29.46 m; (3) LO of *Contusotruncana patelliformis* at 30.51 m.

The overlying stratigraphic interval is assigned to the *C. plummerae* Interval Zone, following the biozonation by Petrizzo et al. (2011) and Gale et al. (2020). In the studied section the LOs of *C. plummerae* and *G. ventricosa* are recorded in the same sample at 29.46 m. According to Petrizzo et al. (2011), *G. ventricosa* shows a diachronous first appearance among different latitudes (mid-high latitudes and low-tropical/subtropical areas) and is very rare at the bottom of its stratigraphic range and very difficult to recognize in thin sections and washed residues. For this reason, instead of the *G. ventricosa* Zone of the standard Tethyan biozonation by Premoli Silva and Sliter (1995) and Robaszynski and Caron (1995), we identify the *C. plummerae* Zone in the interval above 29.46 m of the Čanj section (Fig. 7; Table 1). The lowest occurrence of *C. plummerae* seems to be a much more reliable biozonal marker for the tropical and subtropical area, together with the frequent occurrence of the easily identifiable species *Globotruncanita atlantica* (Petrizzo et al., 2011).

3.4. Isotope stratigraphy

3.4.1. Carbon isotope stratigraphy

Carbon and oxygen stable isotope and Sr isotope profiles obtained for the study section is shown in Fig. 7. Numerical values are listed in Supplementary material S1. The composite carbon isotope curve is constrained by high sample resolution in the middle part of the succession and is poorer in the lower (from 0 to 8 m) and upper parts (above 30 m) of the study section. The average $\delta^{13}C_{carb}$ value for the entire section is 2.49 ‰ with a maximum range of 1 ‰. At the base, from 0 to 3 m, a general positive trend can be observed, with a negative excursion in between having $\delta^{13}C_{carb}$ values around 2.6 ‰, followed by an increase of ~0.5 ‰ to a maximum $\delta^{13}C_{carb}$ value of 3.12 ‰. Above, up to 14 m, the $\delta^{13}C_{carb}$ curve shows a generally strongly decreasing trend towards a minimum of 2.12 ‰ with fluctuations of low amplitude, and a pronounced negative peak value of 2.33 ‰ in between, centered at 8.7 m. From 14 to 19 m, there is a steady, fairly even increase in the $\delta^{13}C_{carb}$ values from 2.12 ‰ to 2.45 ‰. Above this, between 19 and 24 m, the curve shows a succession of positive and negative peaks with $\delta^{13}C_{carb}$ values fluctuating between 2.25 ‰ and 2.66 ‰. In this range of fluctuating values, a positive double peak can be observed, with the value of the first peak being 2.60 ‰ and the second peak 2.66 ‰. Above 24 m the last pronounced negative shift is registered at 25 m with a $\delta^{13}C_{carb}$ value of 2.25 ‰ followed by a positive isotope shift of 0.5 ‰ towards the beginning of RM3. Two positive shifts of ~2.7 ‰ can be seen at 27.5 m and 30 m and coinciding with changes in lithology. In the uppermost part of the section (above 32 m), $\delta^{13}C_{carb}$ values oscillate around a mean value of

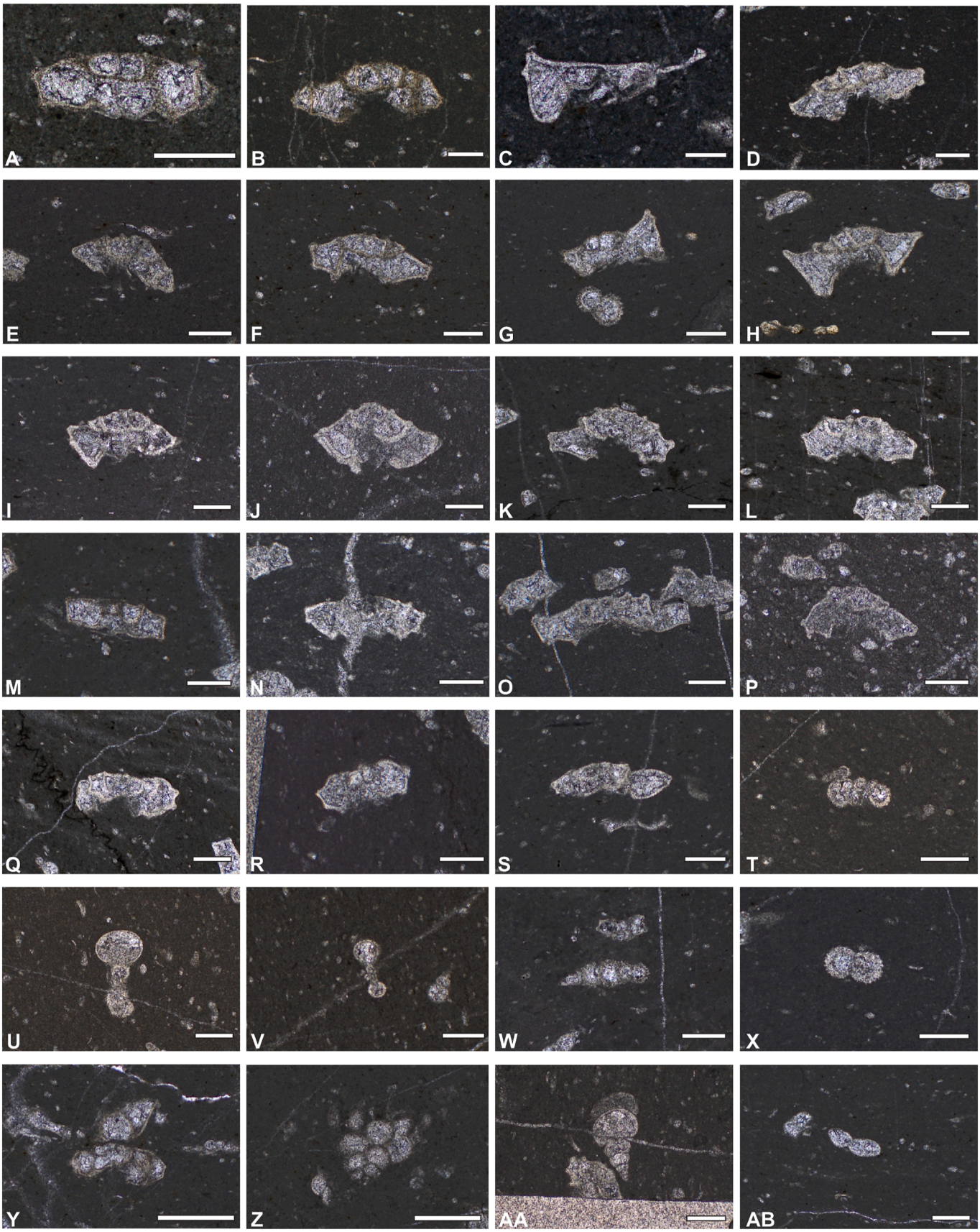

Fig. 6. Selected and most common planktonic foraminifera species from Čanj section. Scale bars = 0.2 mm. (A) *Marginotruncana pseudomarginata*, sample ČN22-6 (13.26 m). (B) *Marginotruncana tarfayaensis*, sample ČN22-06 (13.26 m). (C) *Dicarinella concavata*, sample ČN22-07 (13.41 m). (D) *Marginotruncana coronata*, sample ČN22-08 (13.61 m). (E) *Marginotruncana sigali*, sample ČN22-08 (13.61). (F) *Marginotruncana sinuosa*, sample ČN22-08 (13.61 m). (G) *Dicarinella asymetrica*, sample ČN22-09 (13.85 m). (H)

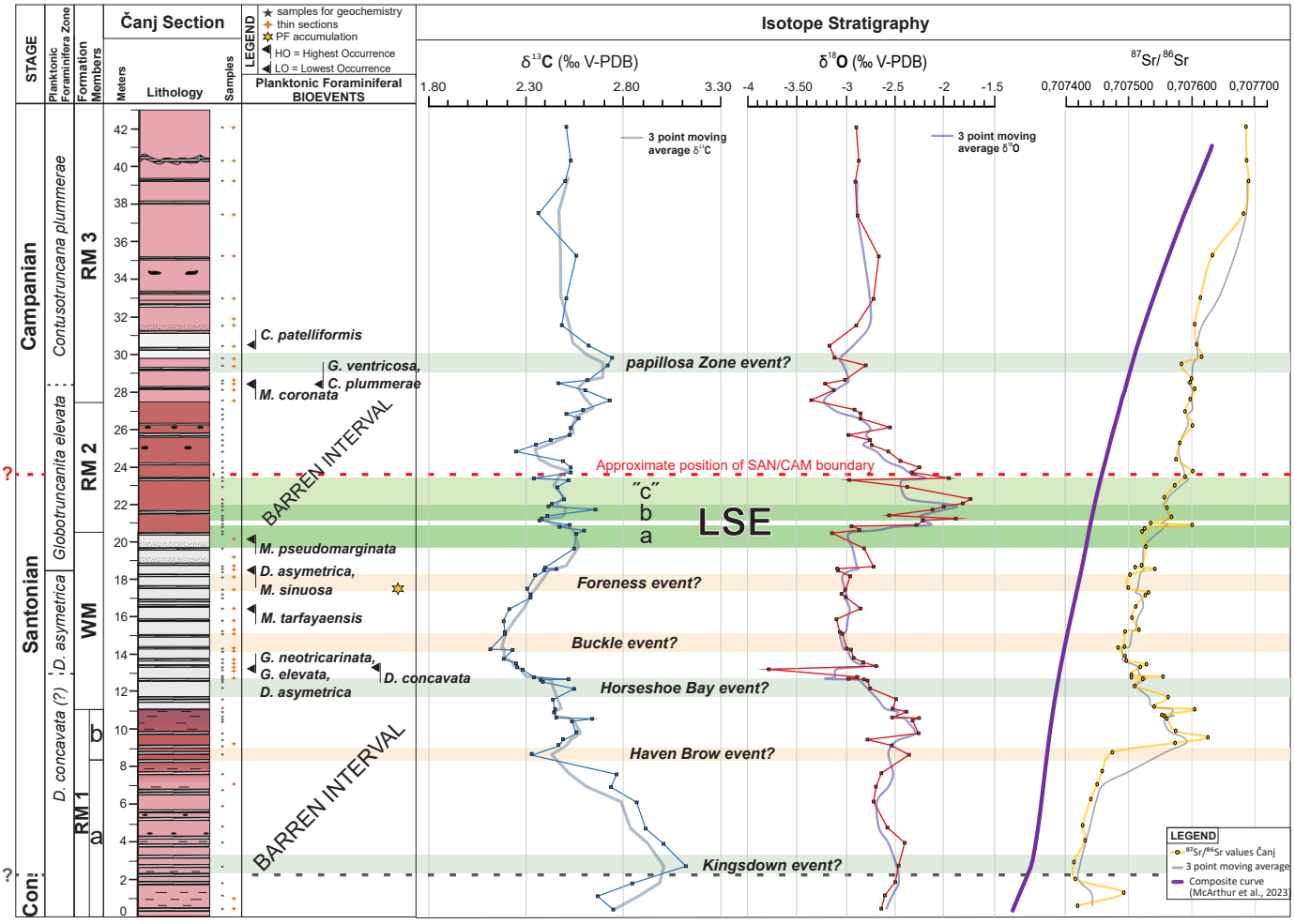

Fig. 7. Lithostratigraphy, $\delta^{13}C_{carb}$ and $\delta^{18}O_{carb}$ stable isotope curves of the Coniacian-Campanian interval of the Čanj section with the distribution of selected planktonic foraminifera. The isotope stratigraphy includes the $^{87}Sr/^{86}Sr$ curve of the Čanj section compared to the composite $^{87}Sr/^{86}Sr$ curve for the Late Cretaceous of McArthur et al. (2024). The position of the Santonian/Campanian boundary is constrained to the top of the positive $\delta^{13}C_{carb}$ excursions of the Late Santonian Event (LSE) revised in Gale et al. (2023), which occurs within the second barren interval of RM2. The Coniacian/Santonian boundary is set below the Kingsdown Event following correlation with the Bottaccione section (see text for explanations and Fig. 11). The carbon isotope events are correlated with the events identified in the Bottaccione section by Thibault et al., (2016), and reference therein (see also Fig. 11). All isotope values from the Čanj section are included in Supplementary material S1.

2.49 ‰ and show a slightly more negative trend towards the top of the succession.

3.4.2. Oxygen isotopes

The oxygen isotope profile for the study section is compared to the carbon and strontium isotope trends in Figure 7. Numerical data are provided in Supplementary material S1. A scatter plot (Appendix 1) of $\delta^{13}C_{carb}$ versus $\delta^{18}O_{carb}$ shows a positive, linear, but very weak ($r = 0.16$; $R^2 = 0.02$) relationship between these two variables, displaying no statistically significant covariance. The oxygen isotope record in the Čanj section is characterized by a general trend towards slightly more negative $\delta^{18}O_{carb}$ values with several pronounced positive excursions. The $\delta^{18}O_{carb}$ values range from a minimum of −3.79 ‰ to −1.76 ‰ and scatter around an average value of −2.72 ‰. In the first 10 m of the section, the $\delta^{18}O_{carb}$ values fluctuate around −2.5 ‰ and change upwards into distinctive lighter trends. Towards the top, the $\delta^{18}O_{carb}$ curve shows a clear drop in values with an average value of −2.89 ‰ and a pronounced negative excursion of −3.79 ‰ which is probably a diagenetic or analytical artifact. At 20.5 m, a negative $\delta^{18}O_{carb}$ value of −3.15 ‰ passes upwards into a large positive shift of 1.39 ‰, which leads to the highest positive $\delta^{18}O_{carb}$ peak value of the section of −1.76 ‰. The trend shifts again towards lower $\delta^{18}O_{carb}$ values and lower fluctuation amplitudes with an average $\delta^{18}O_{carb}$ value of −2.96 ‰.

3.4.3. Strontium isotope stratigraphy

Sr analysis of 71 samples shows a general increasing trend with an $^{87}Sr/^{86}Sr$ ratio ranging from 0.707413 ± 0.000005 at the base of

Globotruncanita elevata, sample ČN22-12 (15.15 m). (I) *Globortuncanita stuartiformis*, sample ČN-16 (17.5 m). (J) *Globotruncanita atlantica*, sample ČN-13 (37.49 m). (K) *Globotruncana arca*, sample ČN22-14 (15.9 m). (L) *Contusotruncana fornicata*, sample ČN22-17 (18.2 m). (M) *Globotruncana linneiana*, sample ČN22-08 (13.61 m). (N) *Globotruncana neotricarinata*, sample ČN22-19 (18.7 m). (O) *Marginotruncana pseudolinneiana*, sample ČN22-11 (14.35 m). (P) *Contusotruncana patelliformis*, sample ČN-12 (35.27 m). (Q) *Globotruncana bulloides*, sample ČN22-17 (18.2 m). (R) *Contusotruncana plummerae*, sample ČN-6 (29.46 m). (S) *Marginotruncana renzi*, sample ČN22-16 (17.5 m). (T) *Muricohedbergella* sp., sample ČN-7 (29.84 m). (U) *Planohedbergella prairiehillensis*, sample ČN-4 (28.48 m). (V) *Laeviella bolli*, sample ČN-6 (29.46 m). (W,X) *Pseudoguembelina* sp., sample ČN22-13 (15.25 m) and ČN22-8 (13.61 m). (Y) *Archaeoglobigerina* sp., sample ČN22-08 (13.61 m). (Z) *Ventilabrella* sp., sample ČN22-10 (14.3 m). (AA) *Pseudotextularia* sp., sample ČN-8 (30.51 m). (AB) *Laeviheterohelix* sp., sample ČN22-14 (15.9 m).

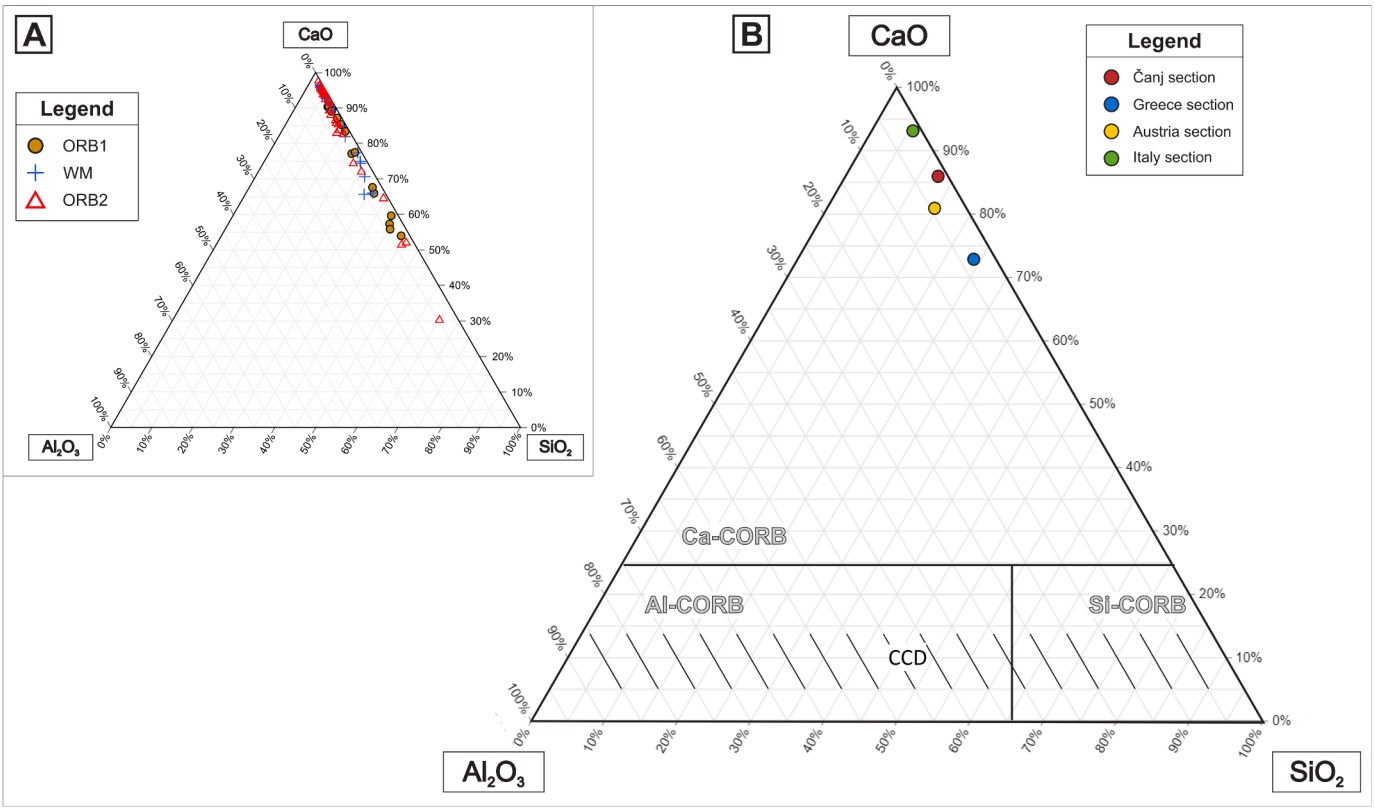

Fig. 8. (A) Ternary diagram representing data clouds of lithostratigraphic units from the Čanj section to estimate the distribution of data and the type of CORB. (B) Ternary diagram for the classification of CORBs (after Wagreich et al., 2009; Hu et al., 2012). The dots in the diagram represent average compositions of comparable Upper Cretaceous sections mentioned in the text and their classification within the CORB system, compared to the geochemical data from the Čanj section in this study. Geochemical data from other sections are from Hu et al. (2012).

the section to 0.707689 ± 0.000005 at the top (Fig. 7; Supplementary material S1). The Sr values initially show a fairly continuous upward increase, but this trend is quickly interrupted by a pronounced increase in values after 8.7 m and a sudden drop at 13.61 m of the section, where the values almost return to the values prior to the sudden rise (about 0.707474 ± 0.000005 before the rise and 0.707496 ± 0.000005 after). The continuous upward rising trend is then interrupted again by an interval from 20.66 m to 27.58 m, within which a further increase in values can be observed. For comparison, an $^{87}Sr/^{86}Sr$ composite reference curve from McArthur et al. (2024) is plotted alongside our data (Fig. 7) from the Coniacian to the Campanian. The curve shows a continuously increasing linear trend expected for the Late Cretaceous, which goes far down from the late Turonian minimum and rises to maximum values in the Maastrichtian (McArthur et al., 2024). However, our data show a consistent offset to higher values relative the composite reference curve that likely reflects overprinting by Sr released from the detrital fraction (Bailey et al., 2000; Li et al., 2020).

3.4.4. CORB's geochemical classification

Intense studies of CORBs (Cretaceous Oceanic Red Beds) began almost two decades ago (Hu et al., 2005, 2012; Neuhuber & Wagreich, 2011; Wang et al., 2009, 2011; and references therein) and represented a completely new window on global oceanic and climatic changes during the Cretaceous greenhouse world. CORBs attract particular attention because they are a type of succession that followed the widespread deposition of organic carbon-enriched deep-sea sediments (Oceanic Anoxic Events, OAEs) in the middle Cretaceous, which was characterized by sedimentation in a dysoxic to anoxic deep-sea environment (Wang et al., 2009). In the case of CORBs, a change from dysoxic/anoxic to oxic deep-sea sedimentation occurred in the Late Cretaceous (and even between OAEs in the middle Cretaceous) with the deposition of pelagic to hemipelagic red shales, red marls, fine-grained limestones (Scaglia-type) and/or red cherts.

This definition of oceanic red beds does not include red sediments formed by erosion or transportation from the continent into the marine environment (Hu et al., 2005). Their common geochemical properties are an extremely low content of organic carbon (usually less than 0.1 % by weight) and a high proportion of iron oxides. The red color is therefore a depositional feature due to sedimentation in a highly oxic bottom environment. CORBs have been found in various basin settings (deep open ocean basins, V-shaped basins or troughs, back-arc basins) and were deposited in middle to low paleolatitudes on both sides of the Tethys, as they outcrop today in the Apennines, the Alps, the Carpathians, Turkey, the Caucasus as well as in the central North Atlantic, the Caribbean and the South Atlantic (Hu et al., 2005). CORBs are defined as a global oceanographic event with a diachronous beginning and termination of the deposition of pelagic red beds, and are assumed to be the consequence of various Earth processes (of local or global scale) and not just climatically driven mechanisms (Hu et al., 2009).

Various studies have shown that CORBs can be divided into three general facies types: red pelagic and hemipelagic carbonates, red deep-water claystones deposited below the Carbonate Compensation Depth (CCD), and red cherts and radiolarites, which were also deposited below the CCD. Based on the geochemical composition of these facies types, a ternary classification was established to characterize the CORBs using CaO, Al_2O_3 and SiO_2

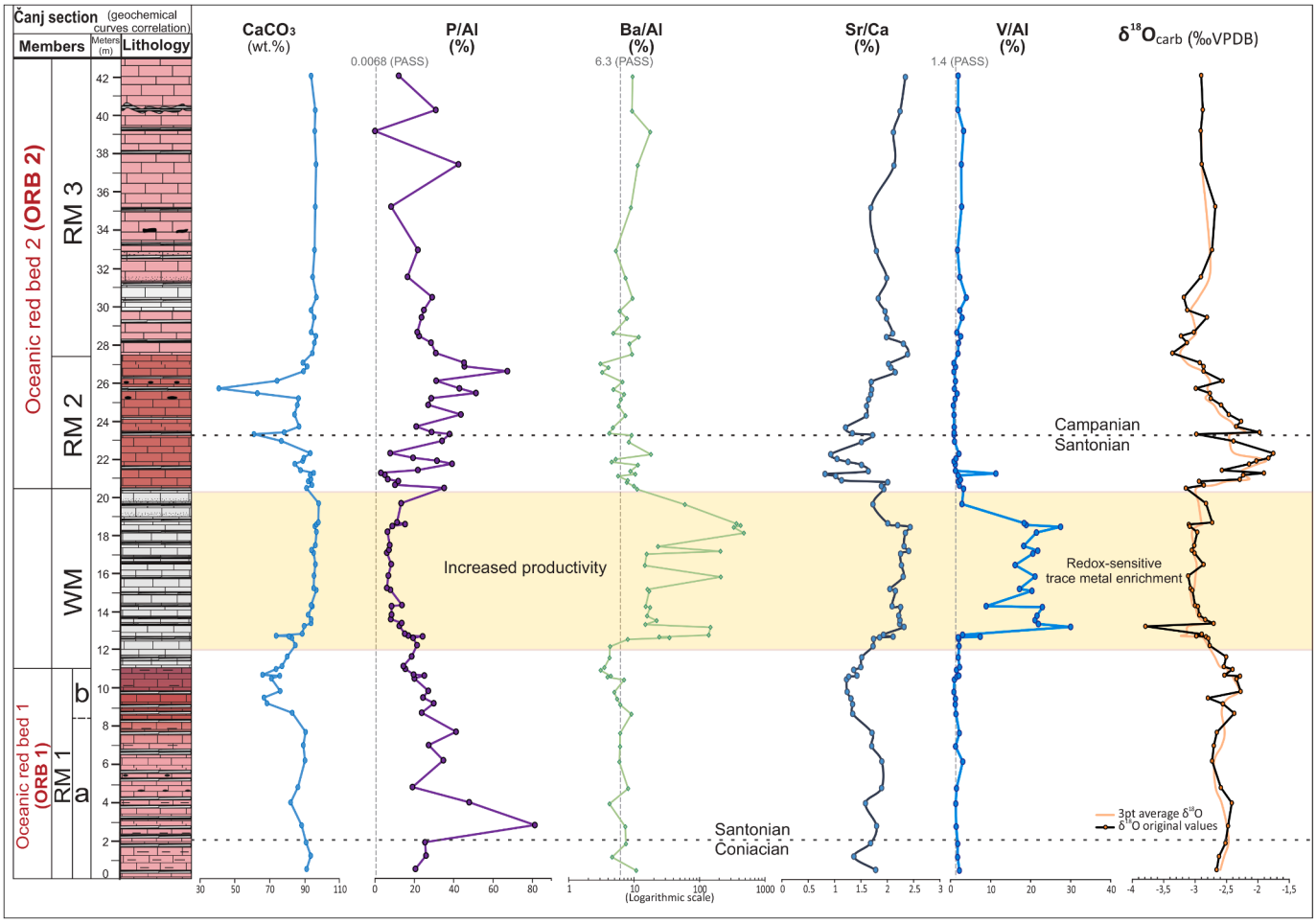

Fig. 9. The distribution of carbonate content, productivity proxies, and selected trace elements are used to assess the degree of paleoproductivity in the Čanj section. Increased productivity proxies and intervals of redox-sensitive proxies are marked with a yellow band. Original data are included in Supplementary material S1.

values as endmembers based on CORB data from numerous publications (Wagreich et al., 2009; Wang et al., 2009; Hu et al., 2012). With this classification, three types of CORBs were defined: carbonate Ca-CORBs, clayey Al-CORBs and siliceous Si-CORBs (Fig. 8). The later classification is based on recent pelagic/hemipelagic sediments as calcareous muds, siliceous muds and red pelagic clays (Hay et al., 1984).

Based on the geochemical data (Supplementary material S1) from the Čanj section, we categorized the studied sequence as a carbonate CORB. The CORB sequence in Čanj is not continuous, but is divided in two different red depositional intervals, ORB1 and ORB2, which are separated by white transitional layers (WM member) (Figs. 3, 4, 7). The $CaCO_3$ content was calculated from the average CaO content of the whole section using an oxide conversion factor of 1.7751 (Hu et al., 2012), based on the assumption that most Ca resides in calcium carbonate. The $CaCO_3$ value is very high at 89.3 %. The value of the second endmember Al_2O_3 reaches 0.8 %, while the SiO_2 content is 7.4 % (Fig. 8; Supplementary material S1). Figure 8 shows two ternary diagrams. The first (Fig. 8A) represents all data (CaO, Al_2O_3, and SiO_2) from the Čanj section and their distribution within the main lithostratigraphic units. The second diagram (Fig. 8B) shows the distribution of different types of CORBs based on average data from various publications in Hu et al. (2012), in addition to the studied section. Looking at their position in the diagram the values of the Čanj section compare very well with other Cretaceous successions deposited in the western Tethys, especially with the Scaglia Rossa Formation in the Vispi Quarry (Gubbio) and Bottaccione section (Umbria-Marche Basin, Italy). The red pelagic limestones/marls of the Scaglia Rossa Formation are also classified as Ca-CORBs with average $CaCO_3$ values of about 95 %, Al_2O_3 values of 0.59 % and SiO_2 content of 3.29 % (Hu et al., 2005, 2012).

Two other Ca-CORB sections with similar $CaCO_3$ contents, but somewhat larger shifts towards the Al and Si end members are the Pindos section in Greece and the Vircgdirf section in Austria (Fig. 8B; Supplementary material S1) (Hu et al., 2012). In these two sections, the average Al_2O_3 content ranges between 2 % and 2.58 %, while the SiO_2 content varies between 8.63 % and 15.73 %. Similar CORBs with higher Si and Al contents are also found in other Austrian sections mentioned by Hu et al. (2012), which were deposited in different paleogeographic domains of the northwestern Tethys: northern passive European margin, middle deep-water Alpine Tethys, southern tectonically active margin of the Adriatic Plate (Wagreich and Krenmayr, 2005; Neuhuber and Wagreich, 2011). The deposition of CORBs in orogenic regions such as the Eastern Alps is therefore much more dynamic and differs from that in the Čanj section, which has no major intercalations of turbiditic input. For this reason, the study of CORBs in this paper will mainly focus on the correlation between the Scaglia Rossa and Čanj sections where sedimentation processes were more mitigated.

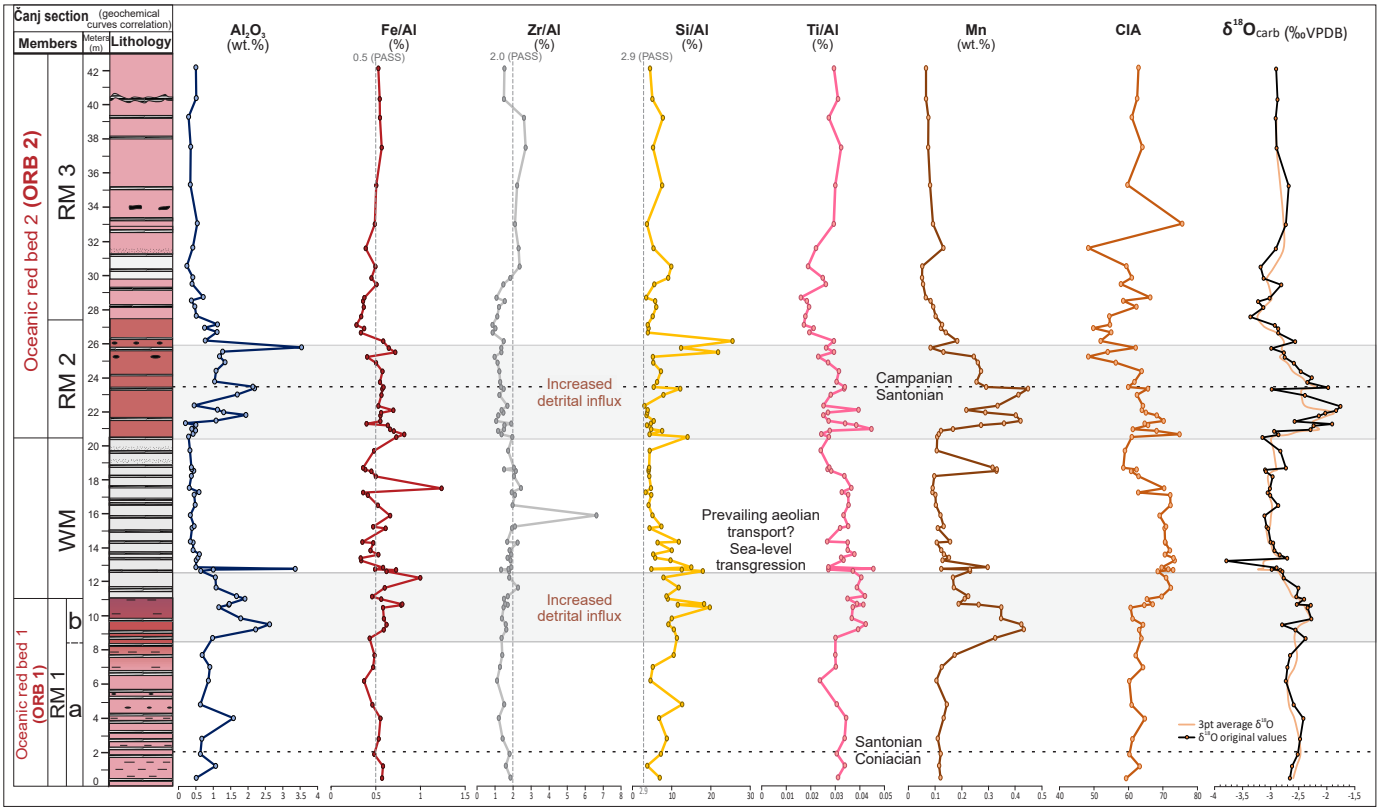

Fig. 10. Distribution of selected major and trace elements, element ratios, Chemical Index of Alteration (CIA) and data on stable oxygen isotopes of the bulk carbonate from the Čanj section. Selected curves provide information on increased detrital input (marked with gray squares) and the intensity of continental weathering during the deposition of the Čanj section. Original data are included in Supplementary material S1.

3.4.5. Elemental geochemistry

The bulk geochemical compositions of the samples from the studied section are presented in Supplementary material S1, while geochemical curves of selected major and minor elements are shown in Figures 9 and 10. The elements are primarily normalized to Al to better assess the element concentrations and enrichment relative to reference marine sediment. Additionally, some element ratios and redox-sensitive trace elements have also been compared to Post-Archean Average Shale (PAAS) values (Taylor and McLennan, 2001).

The average $CaCO_3$ content in the red limestones (ORBs) and the White member (WM; 11 m–20.5 m) is 90.4 % and 86.1 %, respectively. Although the average $CaCO_3$ values do not change significantly between the red and white limestones, the calcium curve in RM1-b and in RM2 shows some conspicuous negative excursions (Fig. 9). These are inversely correlated to the iron (Fe_2O_3) values, which range from 0.06 to 1.73 % with an average value of 0.42 % in the red limestones and are thus significantly higher than in the white limestones, where the Fe_2O_3 values range from 0.09 to 1.25 % with an average value of 0.29 %.

The SiO_2 content of the pelagic sequence is the second highest value within the carbonate CORB. Although the SiO_2 content ranges from 1.06 to 49.6 %, most samples have a silica content of about 3.4 %. Two pronounced positive excursions are found in ORB1 and the lower parts of WM as well as in ORB2, where the SiO_2 content reaches the highest values. The correlation coefficient between SiO_2 and Al_2O_3 shows a positive linear but relatively weak relationship ($r = 0.64$; Appendix 1), while the SiO_2/Al_2O_3 diagram according to Barbera et al. (2006) (Appendix 2) mainly shows a biogenic origin of the silica. The redistributed content of silica due to the dissolution of biogenic shells in the sediment should not be overlooked in this case, nor should the input of detrital silica tied to clay minerals and transported by fluvial or aeolian sources from the adjacent land.

The Al_2O_3 concentrations in Čanj are between 0.20 and 3.54 %, which indicates a general very low input of terrigenous material. Al_2O_3 is positively correlated with Fe_2O_3 and, like the Fe_2O_3 values, has higher positive peaks in ORB1 and ORB2, and lower values around 0.73 % throughout the WM. A similar trend can be observed for TiO_2, K_2O, MgO and Na_2O, which are also detrital-sensitive elements and whose values shift significantly between RMs and WM. The TiO_2 content ranges from 0.004 to 0.14 %, the K_2O content from 0.03 to 0.87 %, the MgO values range from 0.20 to 1.15 %, and the Na_2O values are between 0.02 and 0.44 %. All these major elements have higher values in the ORB1 and ORB2 than in the WM. These elements are also positively correlated with Al_2O_3, with high correlation coefficients for Ti ($r = 0.90$) and K ($r = 0.90$) and slightly lower for Mg ($r = 0.71$) and Na ($r = 0.54$) (all correlation coefficients are found in Appendix 1). The values suggest a common homogeneous source area of detrital input, which apparently did not change significantly during CORB deposition, even during the transition between red and white limestones. The correlation coefficient between Al and Fe is also very high ($r = 0.91$) and follows a close linear relationship, suggesting that the most likely source of iron in this section was terrigenous influx (Neuhuber and Wagreich, 2011). Based on the Fe/Al ratio in comparison to PAAS (Fig. 10), it is likely hosted predominantly in clay and other detrital phases rather than in oxides (Jarvis et al., 2024).

The content of manganese (MnO) in the samples range from 0.05 to 0.45 % and, similar to the lithogenic elements mentioned

above, shows the highest values in the two ORBs, and another conspicuous positive peak is recorded in the upper part of the WM (Fig. 10). In ORB1, the correlation coefficient with Al is moderate ($r = 0.6$), while in ORB2 it is extremely low ($r = 0.18$). This indicates that Mn in the lower part of the section seems to be related to increased detrital/clay input, while the increased Mn values in the upper part could indicate periods of lower bottom water oxygenation. As Mn has a very complex marine geochemistry and is very sensitive to variations in sedimentation rates and biogenic and detrital input, caution should be exercised when interpreting this element in a marine environment (Jarvis et al., 2001; Mansour et al., 2020).

The productivity proxies such as barium (Ba) and phosphorus (P_2O_5) have very low correlation coefficients with Al (Appendix 1) and other detrital input-sensitive elements, so they probably have no common source of origin. P content, normalized to Al to describe its variability in marine sediments (Calvert and Pedersen, 2007), ranges from 0.01 to 0.24 % in the Čanj section, showing elevated values in the lower part of red ORB1 (RM1) and a jagged increasing trend from the WM upwards in the lower parts of ORB2 (during RM2). The jagged increasing values, especially in the ORB parts, could be due to periodic inflow of highly oxygenated, nutrient poor waters as well as reduced sedimentation rates.

The palaeoproductivity proxy Ba and the Ba/Al ratio are often used in studies of pelagic sediments based on normalization to terrigenous elements (such as Al or Ti), as Ba can occur in different mineral phases but is most commonly brought to the sediment as barite (Soua, 2010; Martinez-Ruiz et al., 2015; Schoepfer et al., 2015). The barium values in Čanj vary between 11 and 932 ppm, with the lowest values and an average of 34 ppm in the red limestones. The highest values of Ba are seen in the white limestones reaching a peak of 932 ppm (Fig. 9; Supplementary material S1). This suggests increased primary productivity in the WM and lower productivity in the ORBs. However, in addition to productivity, increased Ba concentrations can also be associated with higher fluvial input into the pelagic environment, which subsequently triggers ocean productivity due to nutrient input, but can also be associated with colder climatic periods or oxygen-rich conditions (Calvert and Pedersen, 2007; Martinez-Ruiz et al., 2015). However, as a redox-sensitive element, Ba enrichment in the WM could indicate primary barite dissolution under moderately reducing conditions near the sediment/water interface (Soua, 2010). This would also be in agreement with low Mn enrichment (Fig. 10), indicating that no oxidation occurred during the deposition of the WM.

3.4.6. CIA weathering index

With the data from the geochemical analysis of some major elements, we were also able to calculate the Chemical index for Alteration (CIA). This index, besides being extremely climate-sensitive, is also used to determine precipitation rates on the source land and serves as a useful tool for further paleoenvironmental interpretation. In the plotted curve (Fig. 10), the higher CIA value represents higher precipitation rates and thus higher weathering intensity (Schöllhorn et al., 2020). Normally, the index is calculated using the formula Al_2O_3 x 100/(Al_2O_3 + CaO + Na_2O + K_2O). However, CaO values are usually replaced with Na_2O to minimize the environmental and diagenetic influence on carbonates (Schöllhorn et al., 2020; Jarvis et al., 2024), which are also the main components of the lithologies in this study. The updated formula is then Al_2O_3 x 100/(Al_2O_3 + 2 x Na_2O + K_2O). The CIA (Fig. 10) shows a relatively stable lower part of the section (ORB1) with smaller shifts in values up to the WM. The latter includes an interval of higher values up to its upper end, where an abrupt decrease follows, followed by higher values again at the beginning of ORB2. After this, the values are quite unstable, falling in the first part of ORB2 (the RM2 member) and rising again relatively sharply towards the upper end of the section. This last rise is interrupted by a marked drop, where white transitional limestones are intercalated between the red limestones of ORB2.

4. Discussion

4.1. Correlation of the Čanj section with other western Tethyan sections (Bottaccione in Italy and Pindos in Greece)

The upper part of the Čanj section in the Budva Basin shows a lithology with similar age and characteristics of the lower Turonian to middle Eocene Scaglia Rossa Formation in the Umbria-Marche Basin (Italy). Like the lithology in the Čanj section, the Scaglia Rossa consists mainly of well-bedded pink to red pelagic limestones (10–30 cm thick) with shale interbeds and frequent stylolites in thicker beds. In contrast to Čanj, the limestones of Scaglia Rossa are rich in calcareous nannoplankton and planktonic foraminifera and benthic specimens are rare (Arthur and Fisher, 1977; Premoli Silva and Sliter, 1995, 1999; Miniati et al., 2020). Based on the presence or absence of chert, the Scaglia Rossa is divided into two members, the lower R1 member (Turonian–lower Campanian) and the upper R2 member (lower Campanian–Maastrichtian) (Alvarez and Montanari, 1988). The lower R1 member consists of chert nodules and chert layers embedded in red to pink limestones, while the upper R2 member is generally free of chert and consists of pink to reddish-brown limestones. Similar lithological changes can be observed in the Čanj section, where the chert content is abundant in the lower part of the section (RM1), while it decreases noticeably towards the top above RM2. Both the Čanj section and the Scaglia Rossa Formation are interpreted as carbonate CORBs with high $CaCO_3$ content (65 %–92 %), very low organic carbon content (less than 0.1 %) and the absence of conspicuous calcareous or terrigenous turbidites and internal structural deformation (Hu et al., 2005; Gale et al., 2023). From a paleogeographic perspective, the Scaglia Rossa developed in the low-latitude pelagic environment of the central western Tethys, similar to the Čanj section, although the latter was located on the eastern edge of the Adriatic platform in a V-shaped basin (Budva Basin) as a northern continuation of the Pindos Basin (Fig. 2).

In the well-preserved Cretaceous deep-water sequences of the Pindos Basin in western Greece, we also find correlative Upper Cretaceous calcareous deposits similar to those in Čanj. Specifically, the lower Coniacian and lowermost Santonian of the Olonos-Pindos Zone are characterized by a transition from red siliceous facies (Katafito Formation) to calcareous deposits (Platy Limestone Formation) (Fleury, 1980; Neumann and Zacher, 2004). This is comparable to Čanj, where a transition occurs from the Bijela Radiolarites to the Scaglia-type red pelagic limestones. In both localities, we can also identify a distinct package of white pelagic limestones that can be correlated to the WM at Čanj and the uppermost Santonian to lower Campanian *Globotruncana* Limestone Member in the Pindos Zone. The Pindos section was also classified as a carbonate CORB, but with higher Al and Si contents (Supplementary material S1). Furthermore, the main difference between the Budva Zone and the Pindos Zone lies in the re-depositional events and turbidite deposits, which are prevalent in the Pindos Basin. These deposits reflect the basin's sensitivity to orogenic events and the tectonic evolution of the northeastern passive margin of the Apulian Plate. This is another reason why we correlate the Čanj section more effectively with the Bottaccione section, as it represents a similar low-latitude Tethyan deep-water

facies without turbiditic deposits, making it a likely analogue for the position of the Santonian/Campanian boundary.

4.2. Identification of the Santonian/Campanian boundary in the Čanj section

The Santonian/Campanian boundary has long been debated and proposed in many sections worldwide, based on various biotic events, isotope stratigraphy, cyclostratigraphy, etc (Wolfgring et al., 2018 and references therein). The Campanian base once defined by ammonites proved problematic due to the rarity and bioprovincialism of these taxa, as did the Last Appearance Datum (LAD) of the crinoid *Marsupites testudinarius* (Schlotheim), which is widespread in shelf successions and chalk facies (Gale et al., 1995) but rare to absent in deep-water sections (Wagreich et al., 2009). Using the LAD of macrofossils as a delineation criterion can be unreliable, as their HOs may be diachronous or poorly sampled between sections, but most problematic can be their rarity in low-latitude pelagic sections (Wagreich et al., 2009). Also not ideal was the solution proposed by Jarvis et al. (2006), who suggested a Boreal/Tethys correlation based on carbon isotope excursions with the definition of the Santonian/Campanian Boundary Event (SCBE), which later proved to be only partially suitable for defining the boundary event (Wendler, 2013; Thibault et al., 2016; Gale et al., 2023).

Subsequently, considering magnetostratigraphy and refined high-precision biostratigraphy as well as isotope stratigraphy, a consensus was reached in 2023 that made the Bottaccione section in Gubbio (Italy) the Global boundary Stratotype Section (GSSP) for the base of the Campanian Stage (Gale et al., 2023). The Santonian-Campanian interval in the Bottaccione section appears to be continuous, providing a detailed microfaunal record for calcareous nannoplankton and planktonic foraminifera, a high-resolution carbon isotope record and a rising strontium isotope record from the bulk sediment. Most importantly, it contains a magnetic polarity reversal from the Long Cretaceous Normal Chron C34n to Chron 33r, which defines the base of the Campanian Stage (Gale et al., 2023).

The studied Upper Cretaceous section in Čanj has not yet been sampled for the primary marker of the Santonian/Campanian boundary, the magnetic polarity reversal from Chron 34n to Chron 33r, but only secondary markers such as planktonic foraminifera and excursions in the $\delta^{13}C_{carb}$ record have been analysed, which could help define the Santonian/Campanian boundary in the Budva Basin zone.

4.2.1. Biostratigraphy and carbon isotope stratigraphy of the Čanj section and correlation with the Bottaccione section

The planktonic foraminifera biostratigraphy incorporates a typical Tethyan Santonian and Campanian planktonic foraminiferal community (Fig. 6; Table 1). The assemblages in the section indicate the uppermost Santonian *Dicarinella asymetrica* Zone, the lower Campanian *Globotruncanita elevata* Zone followed by the *Contusotruncana plummerae* Zone in the upper part of the section. Planktonic foraminifera are not evenly distributed, but their occurrence is interrupted by two large barren intervals (Fig. 7), one in RM1 and below the WM and the second above it in RM2. A large number of planktonic foraminifera typical of the Santonian Stage were found in the WM (from 11 m to 20.5 m). Due to the pronounced barren intervals, we find LOs of many planktonic foraminifera occurring at the same stratigraphic level, which makes difficult to delineate the exact time interval for those bioevents, especially in RM2 and RM3 (Table 1). This applies in particular to the marker species, which are restricted to some levels characterized by poor preservation or coinciding with pronounced changes in lithology. For this reason, the biostratigraphic data from Čanj are correlated, as far as possible, with the positive and negative excursions of the carbon isotope records.

The carbon isotope record seems to be a reliable secondary marker based on the scatter plot of $\delta^{13}C_{carb}$ versus $\delta^{18}O_{carb}$ for all bulk carbonate samples, which shows a weak positive correlation between these two variables that is not statistically significant (Appendix 1). This means that the $\delta^{13}C_{carb}$ record was apparently not significantly affected by diagenesis and the $\delta^{13}C_{carb}$ ratios with short- and long-term trends reflect the changes in the paleoenvironmental carbon isotope signal quite well. Carbon isotopes are much less susceptible to diagenetic alterations and can even maintain first-order trends under the influence of late diagenetic overprinting (Jarvis et al., 2002; Wendler, 2013 and references therein). Foraminifera appear in the section at the base of WM representing the *D. asymetrica* Zone. The HO of *D. asymetrica* is observed in sample ČN22-19 (18.7 m), about 2 m below the base of the second barren interval (RM2). In the WM, the carbon isotope curve reaches the lowest $\delta^{13}C_{carb}$ value at 14.35 m and from this negative excursion, a long-term increase to the upper part of the section begins (Fig. 7). Based on the carbon isotope values and the Santonian foraminiferal assemblage, this rise with several shallow peaks could include two negative carbon isotope events, the lowermost Buckle Event at 14.35 m and the upper Santonian Foreness Event at 18.2 m. The distinct rise between 14.35 m and 21 m ends with two positive peaks that could correspond to the base of the Late Santonian Event (LSE), the positive excursion previously described as the Santonian/Campanian Boundary Event (SCBE) by Jarvis et al. (2002, 2006). Applying the new LSE subdivision according to Jarvis et al. (2023) in the Čanj carbon isotope curve, the interval between 19 m and 25 m would correspond to the carbon isotope peaks LSE-a (19.5–21 m) and LSE-b (21.7–22.7 m) (Fig. 7). The third peak, LSE-c, is less pronounced in our case, as expected in Tethyan regions compared to Boreal chalks (Gale et al., 2023), and since it cannot be precisely delineated on the carbon isotope curve, we have labelled it "c" (Fig. 7). The LSE lies within the barren interval (RM2), so we have no biostratigraphic control in this part of the section to accurately delineate the Santonian/Campanian boundary (Fig. 7). However, when we compare our data with the section in the Bottaccione section (Fig. 11), we see that the LSE-c subevent can be recognized as a positive peak just below the boundary (Thibault et al., 2016; Gale et al., 2023).

The bioevent that lies closest to the LSE in Čanj is the highest occurrence of *D. asymetrica*, an important datum level recognized around the magnetic reversal from C34n to C33r that marks the Santonian/Campanian boundary, but considered diachronous in a more global context (further reading in Gale et al., 2023 and reference therein). In the western Tethys, for example, the HO of *D. asymetrica* in the Bottaccione section is placed at 19.5 cm above the base of Chron C33r (Miniati et al., 2020; Gale et al., 2023), in the NW Tethys, in the Postalm section (Austrian Alps) the HO of *D. asymetrica* is 1.24 m above the base of Chron C33r (Wolfgring et al., 2018), while in Turkey (Wolfgring et al., 2017) the highest occurrence of *D. asymetrica* is 2 m below the base of Chron C33r. Even though this bioevent should be treated with caution at Čanj, as the occurrence of *D. asymetrica* is restricted to the WM only, we cannot exclude that its HO in the section would be even higher if there were no barren intervals. Nevertheless, the distribution range of *D. asymetrica* overlaps with the distribution range of *G. elevata*, which is consistent in the section and defines the *D. asymetrica* Zone below the proposed LSE and the *G. elevata* Zone above it (Fig. 7). Furthermore, a continuous occurrence of *G. elevata* together with *G. stuartiformis* indicates a late Santonian age in the upper part of the *D. asymetrica* Zone.

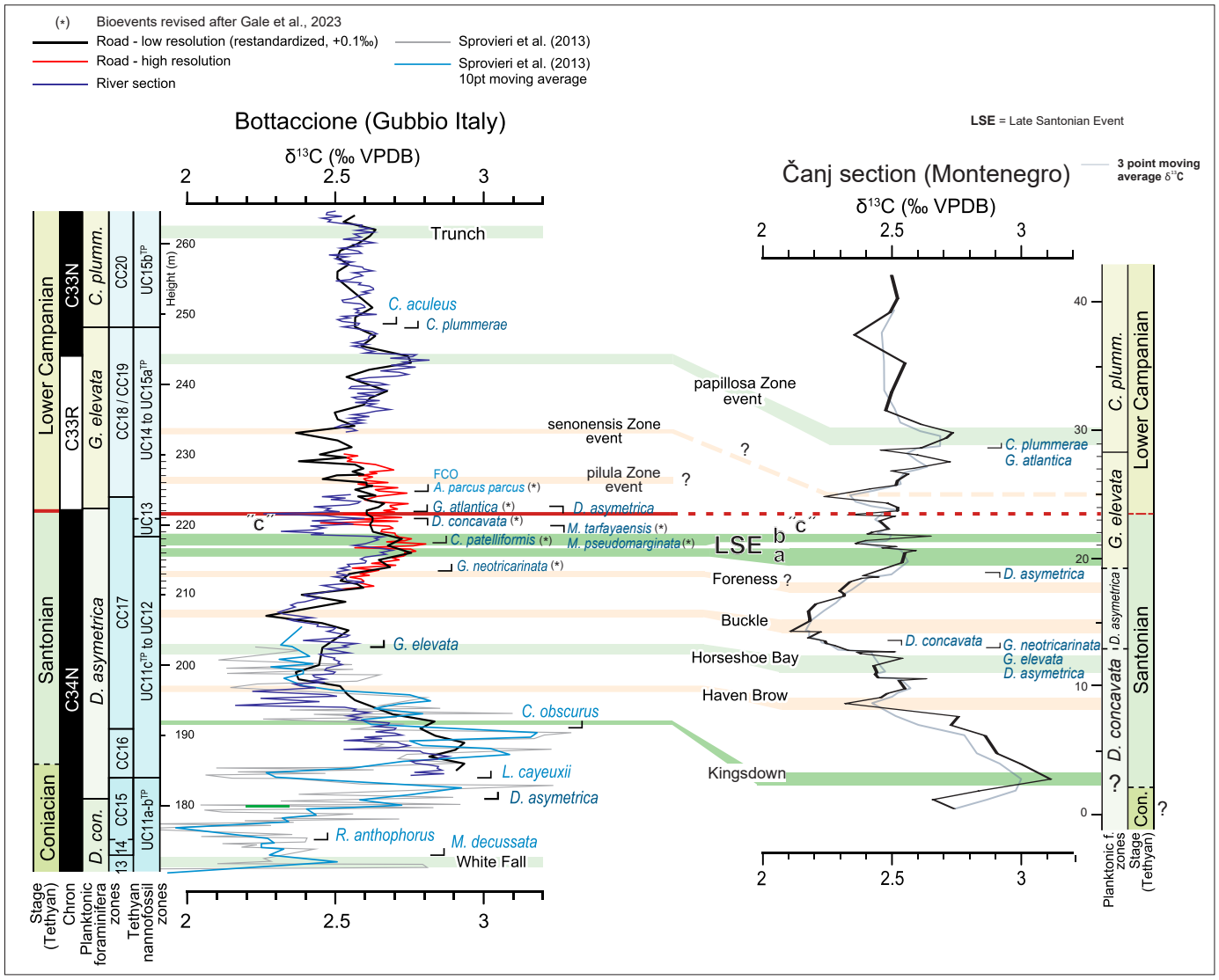

Fig. 11. Correlation of the carbon isotope records and biostratigraphy of the Čanj section with those of the Bottaccione section in Italy as the Tethyan reference for the Upper Cretaceous pelagic carbonate sequence and the GSSP section for the Santonian/Campanian boundary (after Gale et al., 2023). Data of the Bottaccione section are from Thibault et al. (2016), Sprovieri et al. (2013), Gale et al. (2023). Late Santonian Event (LSE) according to Gale et al. (2023), Jarvis et al. (2023), and references therein.

The number of marginotruncanids, abundant throughout the WM, decreases sharply towards the top of the member, together with the HO of *Muricohedbergella flandrini* (Table 1), which is very abundant in the upper Santonian and becomes very rare towards the Campanian (Coccioni and Premoli Silva, 2015). This HO is stratigraphically very close to the HO of *D. asymetrica*. Near the top of the WM (at 17.5 m), there is a curious event within the white limestone in the form of dark grey calcite laminae representing increased abundance of marginotruncanids (Table 1; Fig. 5F, 5H; Fig. 7: yellow star). These laminas occur near the HO of *D. asymetrica* and may represent a sudden foraminifera accumulation of tests that may coincide with fine-grained turbidites or contourites. Based on the data collected in WM and RM2, we estimate the position of the Santonian/Campanian boundary above the potential LSE-"c" to be between 23.5 and 24 m.

RM2 represents not only a distinct lithological change, but also an abrupt break in the microfossil record, probably due to changing environmental conditions in the Budva Basin. Above this break, planktonic foraminifera return, with an abundance of globotruncanids and a disappearance of marginotruncanids, with the exception of *M. coronata*, which was rarely found at the base of RM3 (Fig. 7; Table 1). The record of *G. elevata* is continuous in RM3, although the species richness decreases sharply and, together with the appearance of *C. plummerae*, indicates a shift from the lower Campanian towards the middle Campanian. The LO of *C. plummerae* and its abundant occurrence in the uppermost part of the Čanj section delimit the *C. plummerae* Zone. Above the LO of *C. plummerae* (29.46 m), the carbon isotope curve shows another clear positive shift after the LSE, which according to Sabatino et al. (2018) seems to be characteristic of the early Campanian and occurs at the upper end of Chron 33r and the *G. elevata* Zone. This positive excursion, referred to as the Early Campanian Event (ECE), may be correlated with a prominent positive shift at 30 m in the Čanj section. This shift (Fig. 7, 11) also coincides with the "papillosa Zone event" proposed by Thibault et al. (2016). The *C. plummerae* LO appears slightly below this event in the Čanj section. In the *C. plummerae* Zone, the LO of *G. atlantica* could also be a reliable bioevent, as its occurrence is typical of tropical and subtropical environments of the lower to middle Campanian (Petrizzo et al., 2011).

The lower half of the Čanj section shows a similar situation to the second barren interval in RM2, as here we also have no biostratigraphic control over the carbon isotope curve due to the first barren interval of RM1 (Fig. 7). However, the HO of *D. concavata* at 13.41 m may possibly delineate the lower biozone, the *D. concavata* Zone that extends from the lower part of WM through RM1, although uncertainty remains as to how low this biozone extends due to the barren interval. Towards the base of RM1, the highest positive $\delta^{13}C$ excursion of the Čanj section is recorded at 2.8 m. Similar to Wendler (2013), who compared isotopic data from seven sections from Boreal and Tethyan environments, we observed that the $\delta^{13}C$ increase apparently began in the middle Coniacian, where values remained elevated through the upper Coniacian to the lower Santonian. Thus, if we consider this highest $\delta^{13}C_{carb}$ value in Čanj as part of this general increase, the peak value could correspond to the Kingsdown Event, originally defined in the English Chalk (Jarvis et al., 2006). The lower and more variable values that follow, as part of a longer-term decrease, could represent the negative excursion of the Haven Brow Event at 8.7 m, the medium-term positive carbon excursion of the Horseshoe Bay Event at 12 m, and the previously mentioned lowest negative $\delta^{13}C_{carb}$ excursion of the Buckle Event at 14.35 m in the WM (Fig. 7). The Coniacian/Santonian boundary in the Čanj section fall in the barren interval and it is difficult to correctly place despite the clear change in lithology from RM1-a to RM1-b. However, it could be likely placed below the Kingsdown Event following correlation with the Bottaccione and other Boreal and Tethyan sections (e.g., Wendler, 2013; Thibault et al., 2016) (Figs. 7, 11).

Despite the strong similarity of the carbon isotope curve of Čanj with that of Bottaccione (Fig. 11), it is possible to recognise how much more condensed the sedimentation process was during the deposition of the Čanj succession compared to Bottaccione. Furthermore, this condensed sedimentation in the Budva Basin was apparently interrupted several times by the increased input of terrigenous material and the changing paleoceanographic conditions in the basin, as can be seen from the Čanj sequence, in which different lithologic members appear to be important transitions between different time intervals within the studied section.

4.2.2. Oxygen isotopes

In the stratigraphic log of the Čanj section, the $\delta^{18}O_{carb}$ shifting values appear to be related to the lithologic change or transition from the red beds in the upper part of RM1 to the white beds of the WM and then further on to the red sequence of RM2 (Fig. 7). The shift from white to red pelagic sequences could be a result of the dissolved oxygen content in the bottom water during the sedimentation process in response to changes in paleoclimate (Hu et al., 2005). The $\delta^{18}O_{carb}$ values in Čanj vary between −3.79 ‰ and −1.76 ‰ and are very similar to those reported by Sprovieri et al. (2013) and Sabatino et al. (2018) at Bottaccione, where these low values have been interpreted to reflect increased temperatures during burial diagenesis and/or effects of meteoric diagenesis. The strong diagenetic overprint in Čanj contrasts with the bulk carbon isotope data obtained. Oxygen values nevertheless show a consistent trend, although there is no doubt that early and burial diagenesis occurred with different intensities in the individual members of the Čanj section. Looking at the oxygen curve (Fig. 7), there is a noticeable shift towards higher $\delta^{18}O_{carb}$ values immediately above the top of the WM (20.5 m). The conspicuous positive shift could represent a cooler interval that led to a sea-level lowstand around the Santonian/Campanian boundary, which would correspond to the global onset of a sustained climate cooling from the middle Santonian onwards until the middle Maastrichtian (Miller et al., 2005; Haq, 2014; Wolfgring et al., 2018; Petrizzo et al., 2020, 2022; Mansour and Wagreich, 2022).

However, even though the oxygen curve shows a generally consistent trend, the isotope signal in RM2 is quite noisy, likely due to the strong susceptibility of oxygen isotopes to diagenetic overprinting. In our case, there is significant lithological control, meaning the theory of sustained climate cooling cannot be fully tied to oxygen isotopes. Nevertheless, this cooling event, which marks the transition from a hot to a warm greenhouse, has also been observed in the faunal turnover of planktonic foraminifera. For instance, the transition from the Santonian to the Campanian coincides with the disappearance of marginotruncanids and the proliferation of globotruncanids (Premoli Silva and Sliter, 1999; Petrizzo 2002; Petrizzo et al., 2020). A similar reversal can also be observed in the Čanj section.

4.2.3. Strontium isotopes

The strontium isotope data in the Čanj section were obtained by analysing whole rock carbonate samples. A look at our plotted data (Fig. 7) shows that the curve has a generally increasing $^{87}Sr/^{86}Sr$ trend, which is consistent with the rising values of the marine composite Sr isotope reference curve for the Late Cretaceous (McArthur et al., 2024). However, the rising trend in the strontium curve from the Čanj section is not continuous, but is interrupted by two major disturbances or gaps that strongly influence the Sr signal with abrupt jumps in the Sr values. These two artifacts coincide with the Al enrichments (Fig. 10) in the stratigraphic level of the upper part of the RM1 and the entire RM2 member that could derive from diagenetic or analytical contamination Alternatively, the two artifacts in the Sr curve could be an effect of an increased terrigenic/non-marine input into the pelagic environment and thus a cause for an abrupt increase in Sr values. In any case it is not possible to directly correlate or compare the sample points of the Čanj section with other measured $^{87}Sr/^{86}Sr$ datasets (e.g. with the Postalm section in the Austrian Alps; Wolfgring et al., 2018) or the reference curve of McArthur et al. (2024) against time, as the calculated ages would be shifted. Therefore, assuming that diagenetic or analytical issues are excluded, the steps or jumps in the strontium isotope curve could indicate periods of higher terrigenous input (Fig. 10; Supplementary material S1) rather than intervals of condensed sedimentation, as Sr values on our strontium curve always return to lower pre-fluctuation values.

4.3. Implications for paleoenvironment

4.3.1. CORB deposition in Budva Zone

The deposition of Cretaceous ORBs alone appears to be strongly controlled by low sediment accumulation rates and great paleowater depths, depending in part on the paleogeographic setting. The latter forms the paleobathymetry for circulation in the deep ocean, which is further enhanced by climate cooling episodes in the Late Cretaceous. As the climate cools, more oxic water reaches the sediment/water interface and the efficiency of trapping redox-sensitive nutrients is increased, making the ocean less productive while more oligotrophic/oxic conditions develop (Wang et al., 2009; Hu et al., 2012). These highly oxic conditions and the wide geographic distribution of CORBs suggest an active ocean circulation and the development of cold deep-water connections, that were probably not present in the Early Cretaceous (Hay, 1999; Hu et al., 2005; Wang et al., 2009; Wang et al., 2011). Possible causes for such changes in the ocean/atmosphere system include the reduction of volcanic activity on the seafloor and Cretaceous OAEs, which would lead to a decrease in atmospheric CO_2 and thus to global cooling due to the extensive burial of organic carbon in oceanic basins.

The studied Čanj section represents a carbonate CORB (Ca-CORB) deposited on an outer shelf to the upper/middle bathyal

setting (sensu Hu et al., 2012), in the small V-shaped Budva Basin, which was located in the western Tethys realm (as one of the smaller sub-basins). In our section, there are two ORBs separated by a large package of white transitional limestones (WM member). Elemental geochemical data indicate that the red limestones of ORB1 and ORB2 generally have a similar composition of detrital input-sensitive elements (Al, Ti, K, Mg, Si, Na) and a higher Fe_2O_3 content than the white limestones (Fig. 10; Supplementary material S1), suggesting a similar source area and more oxic conditions at the sediment/water interface. However, some elements or element ratios show significant variations, especially between RM1-b (ORB1) and RM2 (ORB2) (Fig. 10; Supplementary material S1). In these two horizons, $CaCO_3$ content, which is normally relatively high throughout the section, drops abruptly, while Fe content and values of elements related to terrigenous material input show a sudden peak. Fe is often used as a proxy for controlling this type of change in detrital material transport, as it reflects very well short-term changes in the climate system and its influence on the material source area (Wolfgring et al., 2021, and reference therein). Detrital iron could also be a good indicator of increased weathering and increased runoff associated with periods of higher precipitation, but this interpretation is not consistent with CIA values (Fig. 10; Supplementary material S1). It is likely that these two intervals with increased terrigenous input into the basin were not only dependent on climatic changes, but are also a possible consequence of short-term sea-level fluctuations, especially sea-level fall. Manganese is also an element that shows elevated values in the two horizons of the ORBs of the Budva Basin (Fig. 10; Supplementary material S1), but only has a strong correlation with Al in the ORB1 part. This suggests that the high Mn content in RM1-b (ORB1) could be the result of increased terrestrial inflow. This is further supported by a high correlation between Mn and Si ($r = 0.64$; Supplementary material S1) in this part of the sequence. However, since Mn is also a redox-sensitive element, its positive peaks in ORB2 may indicate periods of inflow of highly oxygenated bottom waters. Manganese tends to be better preserved in sediments under oxic conditions, particularly when surface sediments accumulate sufficient Mn oxyhydroxides (Calvert and Pedersen, 2007).

The characteristic red color of the Čanj ORBs is probably due to the oxidizing activity of the cold bottom water masses and the very low sedimentation rates. As also found in the Umbria-Marche Basin in Italy, where the well-known Scaglia Rossa Formation was deposited, the development of oxic bottom conditions could be mainly attributed to tectonic changes that allowed a periodic influx of colder, oxygen-rich bottom waters into sub-basins of the Mediterranean Tethys (Premoli-Silva et al., 1989; Hu et al., 2006).

The low sedimentation rate typical of CORB deposition would therefore provide sufficient time in an oxygen-rich water column for the oxidation of Fe^{2+} to Fe^{3+} (as the main colorant in ORBs), the precipitation of Fe^{3+}-rich oxides in the water column or in/on the surrounding sediment particles, and the incorporation of Fe into the crystal structure of carbonate minerals. This supports the fact that the red coloration of ORBs is a synsedimentary process and not the result of burial diagenesis (Elorza et al., 2021). In addition, the oligotrophic conditions during the deposition of ORB1 and ORB2 are confirmed by geochemical data in the Čanj section and by the absence or low presence of biogenic calcite although the carbonate may derive by recrystallized calcareous ooze and planktonic foraminifera. The low primary productivity in this case is supported by a low Ba content, a slightly lower $CaCO_3$ content compared to the white limestones and an increased P content (Fig. 9). The latter is typically recycled to seawater during anoxic/euxinic conditions, which increases productivity, but in oxygen-rich ocean water the efficiency of phosphorus fixation increases, leading to less productive and more oxic conditions in the deep sea (Colman and Holland, 2000; Calvert and Pedersen, 2007; Wang et al., 2009). Towards the top of ORB1, the pink limestones witch into darker red and purple limestones of the RM1-b member (Fig. 4E). This transition could be attributed to several factors, including changes in sedimentation rates, which may result from high fluvial input and increased proximity to detrital sediment sources. Additionally, variations in oxygen content near the sediment/water interface, influenced by shifting Oxygen Minimum Zones (OMZ), as well as the behaviour of redox-sensitive elements, could also play significant roles in this color transition (Soua, 2010; Elorza et al., 2021).

In contrast to the ORBs, the geochemical results of the WM show a lower content of terrigenous elements and a relatively high $CaCO_3$ and Ba content, which indicates an increased primary productivity. The change in color of the pelagic sediment could be the result of a reduced oxidation capacity of the water masses due to higher temperatures, sea-level transgression or change in sedimentation rates. The incorporation of organic carbon would therefore be higher compared to the red limestones, which would lead to reducing conditions at the sediment-water interface. Under increased redox conditions or with a high influx of organic matter, Fe^{2+} can be released into the water column and subsequently precipitate as pyrite (FeS_2) (Elorza et al., 2021). In our case, it is possible that a small amount of pyrite precipitation occurred within the white limestones. This process could explain the presence of opaque residues or fillings observed in the chambers of the foraminifera shown in Fig. 5H. The increased productivity in surface waters could have been triggered by an increased nutrient supply in the basin. The CIA weathering curve also shows a persistent positive shift within the white limestones, as does the oxygen isotope curve, indicating a slightly warmer climate during the sedimentation interval of the WM. Another process that may have contributed to the formation of white limestones is the prolonged absence of occasional inflow of cold, oxygen-rich bottom water, which was influenced not only by changes in the climate-ocean system, but also by sea level changes indirectly connected to tectonic activity and changes in basin topography (Hay et al., 1999). A possible scenario is that the deposition of the WM may have been influenced by a temporary restriction of the basin, leading to reduced bottom-water ventilation. This restriction could have created a more isolated or stagnant environment, potentially affecting the oxygen levels and overall geochemical conditions within the basin.

4.3.2. Foraminifera change and environment

Certainly, there are many processes that could have acted simultaneously to contribute to the deposition of such a thick package of white limestones between the sedimentation of the lower ORB1 and ORB2 of the Čanj section. What is certain is that the ORB1 and the beginning of the ORB2 represent two perturbances that initiated and terminated the deposition of the white limestones and somehow influenced bioproductivity at that time. The oxygen isotope curve shows a change from a relatively warm period during the deposition of the WM towards a cooler climate situation (Fig. 7). This would fit with the beginning of a cooling phase at the Santonian/Campanian boundary, which also represents a period of increased global deposition of CORB (Neuhuber and Wagreich, 2011). This change is also noticeable in the foraminifera assemblages in the white limestones of WM and later in the upper part of ORB 2 (RM3). The transition from a hot to a warm greenhouse in the Santonian and early Campanian affected globally all trophic groups of planktonic foraminifera, suggesting that changes occurred throughout the water column, which began to

stratify, supporting the theory of altered deep-water circulation (Premoli Silva and Sliter, 1999).

Marginotruncanids are abundant in the white limestones (WM) and represent a double-keeled mesotrophic group that became extinct in the latest Santonian and early Campanian (Petrizzo, 2003; Petrizzo et al., 2020). Meanwhile, the more complex double-keeled genera *Globotruncanita* and *Globotruncana* began to thrive, favouring more stable, oligotrophic environments (Premoli Silva and Sliter, 1999; Petrizzo et al., 2020). The foraminiferal assemblages in ORB 2 in Čanj, therefore, contain very few remnants of marginotruncanids and no dicarinellids. However, this Campanian interval includes foraminifera with highly diversified globotruncanids, *Contusotruncana* species, and rare smaller, unkeeled opportunistic taxa that exhibit a higher degree of adaptation to different trophic regimes. This would be consistent with the generally accepted model of the onset of the cooling phase from the late Santonian to the early Campanian (Petrizzo et al., 2022) and also with the increased deposition of CORB. The incipient cooling of the surface ocean apparently favored the distribution of cooler/deep-dwelling globotruncanids and negatively impacted the shallower *Marginotruncana* and *Dicarinella* species that evolved during the hot greenhouse interval in the Turonian and Coniacian (Premoli Silva and Sliter, 1999; Falzoni et al., 2016; Petrizzo et al., 2020). These compositional changes have been documented at various low to high latitudes sites, although they do not occur simultaneously at all locations (Petrizzo et al., 2020, 2022; and reference therein), which is very similar to the diachronic occurrence of Cretaceous ORBs worldwide.

4.3.3. Elemental proxies linked to sea-level changes

In the pelagic successions, the determination of sea-level fluctuations can be complicated by several facts, such as high depositional water depths, indistinct lithofacies changes compared to coastal areas and carbonate platforms, material from different source areas overprinting each other, etc. (see Wagreich et al., 2020). The Čanj section is generally a homogeneous section of strongly lithified pelagic limestones without conspicuous changes in lithology, such as the presence of marl/limestone or chert/shale couplets and coarser-grained sediment input to accurately define sea-level changes or distinct climatic cycles (Haq, 1993, 2014; Wagreich et al., 2020). However, the geochemical data presented (Supplementary material S1; Figs. 9, 10) provide good evidence for sea-level changes based on some chemical proxies associated with terrigenous siliciclastic input, indicating periods of relative sea-level lowstand or regressions.

Two intervals in the Čanj section show pronounced pulses of terrigenous input with an increase in major elements and some trace elements: RM1-b (ORB1) and the lower part of RM2 (ORB2) (Fig. 10; Supplementary material S1). In both intervals, the Al content, which typically reflects clay abundance in mudstones (LaGrange et al., 2020), is increased together with other clay mineral elements (Fe, Mg, K), which correlate strongly with Al indicating a common area of origin. A further increase in values can be observed for detrital-heavy mineral associated trace elements like Ti and Zr, which also correlate positively with Al. Elevated values of these chemical proxies in pelagic sediments indicate increased current energy and siliciclastic input from land. While the Zr/Al ratio likely reflects changes in coarse sediment supply, the Ti/Al ratio can be used to track proximity to detrital sediment sources and variations in relative sea level (LaGrange et al., 2020). The content of Ti and Zr in the pelagic environment varies strongly depending on weathering, but also on the intensity of aeolian transport (Chen et al., 2013; Martinez-Ruiz et al., 2015; Wagreich et al., 2020). Therefore, these trace elements may be more strongly associated with climate change than with sea-level fluctuations (Wagreich et al., 2020; Wendler et al., 2016). Manganese is another element that shows higher values in RM-b and RM2. The high Mn content in RM1-b (Fig. 10; Appendix 1) is mainly determined by the input of terrigenous detritus, as it correlates relatively strongly with Al, while the correlation in RM2 is only weakly pronounced. In RM2, the high Mn content could be related to the increased oxygenation of the bottom water masses or the input of organic matter, as Mn is related to sedimentation rates and detrital supply, but may also be a carbonate-bound element (Jarvis et al., 2001; Mansour et al., 2020). In terms of sea-level fluctuations, increased Mn content can coincide with transgressive phases, leading to a decrease in values during the late highstands, but can also be abundant during transgressive phases due to increased productivity during sea-level rise (Renard et al., 2007; Wagreich et al., 2020). In contrast, high concentrations of Al and accompanying terrigenous elements are inversely correlated with $CaCO_3$ concentrations (Fig. 9, 10), which would confirm minor/local regression or lowstand phase during deposition of RM1-b and the lower part of RM2.

A transgressive phase or highstand is observed in the WM with increased $CaCO_3$ content, planktonic foraminifera and productivity proxies such as Ba and Ba/Al ratio. Furthermore, Ti/Al and Si/Al are often regarded as markers for aeolian detrital supply especially in transgressive setting (Soua, 2010; LaGrange et al., 2020), which is consistent with the transgressive phase during the deposition of the WM, where the detrital fraction in Figure 10 is likely predominantly aeolian. In addition, transgressive intervals can be characterized by higher amounts of organic material and the admixture of redox-sensitive elements such as vanadium (Wagreich et al., 2020), the concentration of which increases in the WM (Fig. 9). Vanadium can become enriched in anoxic to euxinic environments and can be a further indicator of transgressive phases (LaGrange et al., 2020). Higher values can also be observed for the Sr/Ca ratio in the same member. Strontium, like manganese, has a complex marine geochemistry controlled by many factors, but is often used as a proxy for sea level reconstruction, particularly normalized in respect to Ca (Li et al., 2000; Jarvis et al., 2008). The Sr/Ca ratio is used to infer relative sea level changes, with lower values of the Sr/Ca ratio consistent with transgressions, while higher values correspond to regressive phases or lowstands when Sr-rich shallow-water carbonates are heavily weathered and more Sr is introduced into the deep pelagic environment (Li et al., 2000; Wagreich et al., 2020). In the Čanj section, a plateau with elevated Sr/Ca ratio values (Fig. 9) in the WM is likely related to productivity, as the Sr/Ca ratio of pelagic carbonates can be influenced not only by erosion of former platform carbonates, but also by productivity variation (Jarvis et al., 2008). In other parts of the section, the Sr/Ca ratio does not show similar long-lasting increases, but rather short-term increases that may coincide with a rapid decline in sea level and an increase in the Sr/Ca ratio of seawater (Jarvis et al., 2008 and reference therein). The rapid fluctuations in Sr/Ca ratio values in RM2 could also be due to the increased influx of terrigenous material compared to that supplied by carbonate platforms.

During the ice-free greenhouse periods of Earth's history, changes in sea-level may have been influenced by different processes than during the icehouse times. An example of this is the oxygen isotope record, which is excellent for deciphering sea-level changes during cool periods, as the continental ice caps were the main mechanism for sea level changes. On the other hand, $\delta^{18}O_{carb}$ values may show different trends during hot/warm greenhouse periods and therefore cannot be directly used to decipher sea-level changes under such climate conditions, but need to be combined with other proxies (Wagreich et al., 2020). During greenhouse phases, sea-level fluctuations in pelagic and hemipelagic deposits

depend mainly on grain size and siliciclastic input and apparently on another important process such as aquifer-eustasy (Wendler et al., 2016; Wagreich et al., 2020; Sames et al., 2020). Considering the aquifer-eustasy model (Sames et al., 2020) and the increase of terrigenous material (and leading chemical proxies) in our study, we can interpret the Čanj section as follows: After the deposition of RM1-a, which seems to occur during a phase of rather higher relative sea-level, the deposition of RM 1-b could represent a period of humid climate, low sea-level and higher input of siliciclastic material. This phase appears to have been interrupted by a change to an arid-warm climate (deposition of the WM) in which transgression and high sea-level due to aquifer discharge prevailed (Wendler et al., 2016; Sames et al., 2020). Continental weathering would decrease at this time due to the drier climate, and aeolian transport of weathered Al-rich minerals and Si may have been the main transport process. However, the chemical alteration index (CIA) shows relatively high values for the WM (Fig. 10), suggesting a wetter climate during the deposition of the white limestones. In contrast, the Ti/Al ratio, being another good indicator of aeolian transport (Chen et al., 2013), also shows elevated values during the same period, suggesting that Al-rich minerals were transported by wind over longer distances into the open sea. Since the Al-rich minerals are mainly clays associated with enhanced weathering, the high CIA values in this interval could be related to a period of intense weathering on the continent, while the resulting weathered material was later transported by the wind. The increase in biogenic component in this interval also supports the theory of a transgressive phase, in which typically larger amounts of terrestrial organic matter and debris are transported from vast coastal plains, swamps and deltas to the sea (Mansour and Wagreich, 2022).

The next red member RM2 again shows an increased input of terrigenous material, indicating another interval of lower sea-level and more humid climate, which could have been shorter and less pronounced here, especially around the Santonian/Campanian boundary.

The oxygen isotope values in warm and humid greenhouse intervals would represent periods of increased ^{16}O-rich groundwater input from land rather than a very strong cold climate pulse as in an icehouse world. However, a possible influx of colder water masses into the pelagic environment of the Budva Basin should not be neglected, which could be evidenced by a change in foraminifera composition and sudden deposition of CORB. Furthermore, different findings (Davies et al., 2020; Davies and Simmons, 2024) argue against aquifer-eustasy generating observable transgressions. They suggest that glacio-eustasy was the dominant driver of short-term Cretaceous sea-level changes, while aquifer-eustasy had a significantly smaller impact. Higher CO_2 levels could have increased global precipitation but did not significantly alter arid and humid conditions to account for sea-level changes.

Further analysis of clay mineralogy, particularly the ratio of kaolinite to illite, should be carried out to provide detailed evidence of alternating humid and arid climate episodes associated with sea-level changes.

5. Conclusions

This study offers a detailed examination of the Upper Cretaceous basin sequence in the Čanj section and provides new insights into the evolutionary framework of the western Tethys realm, with a focus on the Budva Basin (Dinarides) in Montenegro. Using an integrated stratigraphic approach that incorporates biostratigraphy, carbon isotope stratigraphy, and geochemical data, we have identified the Santonian/Campanian boundary and several carbon isotope excursions. The data also revealed a very good correlation to the carbon isotope curve from the Bottaccione section (Italy), despite the much lower sedimentation rate observed in the Čanj section. The analysis of planktonic foraminifera revealed key biostratigraphic taxa, such as the highest occurrence of *Dicarinella asymetrica* in the White Member (WM), further supporting the placement of the Santonian/Campanian boundary. Two barren intervals lacking planktonic foraminifera were associated with paleoenvironmental disturbances that correspond to significant geochemical shifts within the 42-m-thick pelagic limestone sequence.

Variations in elemental concentrations correlate principally with lithological changes, interpreted to correspond to paleoceanographic shifts, such as long-term sea-level fluctuations, rather than short-term climatic changes. A possible aquifer-eustasy model, based on the warm Late Cretaceous greenhouse climate, is considered in interpreting the geochemical and oxygen isotope data as well as sea-level fluctuations. Moreover, the occurrence of warm-temperate, low-latitude Tethyan planktonic foraminifera species during this time suggests a transgressive eustatic sea level, further reinforcing the climate-based connection to sea level fluctuations.

A comparative analysis with similar Cretaceous Oceanic Red Beds (CORBs) from the Mediterranean and the Bottaccione section highlights the regional significance of the Čanj section. The data gathered enhance our understanding of depositional environments and biotic responses during the Late Cretaceous, offering a more comprehensive view of the evolution of the Budva Basin.

CRediT authorship contribution statement

Anja Kocjančič: Writing – original draft, Visualization, Methodology, Investigation, Conceptualization. **Maria Rose Petrizzo:** Writing – review & editing, Methodology. **Aleksander Horvat:** Writing – review & editing, Supervision, Resources, Project administration, Methodology, Funding acquisition, Conceptualization.

Declaration of competing interest

The authors declare the following financial interests/personal relationships which may be considered as potential competing interests: Anja Kocjančič reports financial support was provided by Slovenian Research and Innovation Agency. Aleksander Horvat reports financial support was provided by Slovenian Research and Innovation Agency. If there are other authors, they declare that they have no known competing financial interests or personal relationships that could have appeared to influence the work reported in this paper.

Acknowledgments

The authors are indebted to Ian Jarvis and Andy Gale for their thoughtful suggestions that greatly improved the final version of the manuscript. The Associate Editor Ottilia Szives is thanked for the editorial work. This study was carried out with the financial support of the Slovenian Research and Innovation Agency (ARIS) within the research programme P1-0008. We thank Dr. Sylvia Riechelmann (Ruhr-Universität Bochum) for sample preparation and performing Sr isotope ratio analysis. We thank Dr. Attila Demény (Research Centre for Astronomy and Earth Sciences Budapest) for sample preparation and measurements of carbonate

samples for stable carbon and oxygen isotopes. We thank Dr. John M. McArthur (University College London) for valuable comments and guidelines for Sr isotope interpretations and the latest personal database of Sr isotope curves and ratios. We are grateful to Dr. Martin Đaković (Geological Survey of Montenegro) for his knowledge and assistance during fieldwork, and to Dr. Špela Goričan (Research Centre of the Slovenian Academy of Sciences and Arts) for all the help and knowledge in fieldwork, critical reading and suggestions for this article.

Data availability

All data are available in the article.

References

Alvarez, W., Montanari, A., 1988. The Scaglia limestone (Late Cretaceous–Oligocene) in the northeastern Apennines carbonate sequence: stratigraphic context and geological significance. In: Premoli, Silva I., Coccioni, R., Montanari, A. (Eds.), The Eocene–Oligocene boundary in the Marche–Umbria basin (Italy), vol. 1. Industrie Grafiche F.lli Aniballi, Ancona, pp. 13–29.

Arthur, M.A., Fischer, A.G., 1977. Upper Cretaceous–Paleocene magnetic stratigraphy at Gubbio, Italy. Lithostratigraphy and sedimentology. Geological Society of America Bulletin 88, 367–371.

Bailey, T.R., McArthur, J.M., Prince, H., Thirlwall, M.F., 2000. Dissolution methods for strontium isotope stratigraphy: whole rock analysis. Chemical Geology 167, 313–319.

Barbera, G., Mazzoleni, P., Critelli, S., Pappalardo, A., Lo Guidice, A., Cirrincione, R., 2006. Provenance of shales and sedimentary history of the Monte Soro Unit, Sicily. Periodico di Mineralogia 75 (2–3), 313–330.

Cafiero, B., De Capoa Bonardi, P., 1980. Stratigraphy of the pelagic Triassic in the Budva-Kotor area (Crna Gora, Montenegro, Yugoslavia). Bolletino della Societa Paleontologica Italiana 19 (2), 179–204.

Cafiero, B., De Capoa Bonardi, P., 1981. I Conodonti dei calcari ad Halobia del Trias superior del Montenegro (Crna Gora, Jugoslavia). Rivista Italiana di Paleontologia 86 (3), 563–576.

Calvert, S., Pedersen, T.F., 2007. Chapter Fourteen Elemental Proxies for Palaeoclimatic and Palaeoceanographic Variability in Marine Sediments: Interpretation and Application. Developments in Marine Geology 1, 567–644. https://doi.org/10.1016/S1572-5480(07)01019-6.

Chen, Huei-Fen, Yeh, Po-Yi, Song, Sheng-Rong, Hsu, Shih-Chieh, Yang, Tien-Nan, Wang, Yong, Chi, Zhenqing, Lee, Teh-Quei, Chen, Min-Te, Cheng, Chien-Liang, Zou, Jianjun, Chang, Yuan-Pin, 2013. The Ti/Al molar ratio as a new proxy for tracing sediment transportation processes and its application in aeolian events and sea level change in East Asia. Journal of Asian Earth Sciences 73, 31–38. https://doi.org/10.1016/j.jseaes.2013.04.017.

Colman, A.S., Holland, H.D., 2000. The global diagenetic flux of phosphorus from marine sediments to the oceans: redox sensitivity and the control of atmospheric oxygen levels. In: Glenn, C.R., Prévôt-Lucas, L., Lucas, J. (Eds.), Marine Authigenesis: from Global to Microbial, Soc. Econ. Paleont. Mineral., vol. 66. Spec. Publ., pp. 53–75. https://doi.org/10.2110/pec.00.66.0053

Črne, A.E., Weissert, H., Goričan, Š., Bernasconi, S.M., 2011. A biocalcification crisis at the Triassic–Jurassic boundary recorded in the Budva Basin (Dinarides, Montenegro). GSA Bulletin 123 (1–2), 40–50.

Danilova, A., 1958. Mikropaleontološki prikaz zona višeg senona u Boki Kotorskoj. Geološki glasnik. Titograd 11 (223–232), 23–27.

Davies, A., Simmons, M.D., 2024. Placing constraints on the nature of short-term eustatic curves. Basin Research 36, e12832. https://doi.org/10.1111/bre.12832.

Davies, A., Gréselle, B., Hunter, S.J., Baines, G., Robson, C., Haywood, A.M., Ray, D.C., Simmons, M.D., van Buchem, F.S.P., 2020. Assessing the impact of aquifer-eustasy on short-term Cretaceous sea-level. Cretaceous Research 112, 104445. https://doi.org/10.1016/j.cretres.2020.104445.

Elorza, J., Gómez-Alday, J.J., Jiménez Berrocoso, A., 2021. Syndepositional processes in the pigmentation of oceanic red beds: evidence from the Basque–Cantabrian Basin (northern Spain). Geological Magazine 158 (9), 1683–1703. https://doi.org/10.1017/S0016756821000248.

Falzoni, F., Petrizzo, M.R., Jenkyns, H.C., Gale, A.S., Tsikos, H., 2016. Planktonic foraminiferal biostratigraphy and assemblage composition across the Cenomanian–Turonian boundary interval at Clot Chevalier (Vocontian Basin, SE France). Cretaceous Research 59, 69–97. https://doi.org/10.1016/j.cretres.2015.10.028.

Fleury, J.J., 1980. Les zones de Gavrovo–Tripolitza et du Pinde–Olonos (Grèce continentale et Péloponnèse du Nord). Evolution d'une plateforme et un bassin dans le cadre alpin. Société Géologique du Nord 4, 651.

Gale, A.S., Mutterlose, J., Batenburg, S., Gradstein, F.M., Agterberg, F.P., Ogg, J.G., Petrizzo, M.R., 2020. Chapter 27 - The Cretaceous Period. In: Gradstein, F.M., Ogg, J.G., Schmitz, M.D., Ogg, G.M. (Eds.), Geologic Time Scale. Elsevier, pp. 1023–1086. https://doi.org/10.1016/B978-0-12-824360-2.00027-9, 2020.

Gale, A.S., Batenburg, S., Coccioni, R., Dubicka, Z., Erba, E., Falzoni, F., Haggart, J., Hasegawa, T., Ifrim, C., Jarvis, I., Jenkyns, H., Jurowska, A., Kennedy, J., Maron, M., Muttoni, G., Pearce, M., Petrizzo, M.R., Premoli-Silva, I., Thibault, N., Voigt, S., Wagreich, M., Walaszczyk, I., 2023. The Global Boundary Stratotype Section and Point (GSSP) of the Campanian Stage at Bottaccione (Gubbio, Italy) and its Auxiliary Sections: Seaford Head (UK), Bocieniec (Poland), Postalm (Austria), Smoky Hill, Kansas (U.S.A), Tepayac (Mexico). Episodes 46, 451–490. https://doi.org/10.18814/epiiugs/2022/022048, 2023.

Goričan, Š., 1994. Jurassic and Cretaceous radiolarian biostratigraphy and sedimentary evolution of the Budva Zone (Dinarides, Montenegro). Memoires de Geologie Lausanne 18, 177.

Goričan, Š., Đaković, M., Baumgartner, P.O., Gawlick, H.J., Cifer, T., Djerić, N., Horvat, A., Kocjančič, A., Kukoč, D., Mrdak, M., 2022. Mesozoic basins on the Adriatic continental margin–a cross-section through the Dinarides in Montenegro/Mezozojski bazeni na kontinentalnem robu Jadranske plošče–presek čez Dinaride v Črni gori. Folia biologica et geologica 63 (2), 85–150.

Handy, M.R., Ustaszewski, K., Kissling, E., 2015. Reconstructing the Alps–Carpathians–Dinarides as a key to understanding switches in subduction polarity, slab gaps and surface motion. International Journal of Earth Sciences 104, 1–26. https://doi.org/10.1007/s00531-014-1060-3.

Haq, B.U., 1993. Deep-Sea Response to Eustatic Change and Significance of Gas Hydrates for Continental Margin Stratigraphy. In: Posamentier, H.W., Summerhayes, C.P., Haq, B.U., Allen, G.P. (Eds.), Sequence Stratigraphy and Facies Associations. https://doi.org/10.1002/9781444304015.ch6.

Haq, B.U., 2014. Cretaceous eustasy revisited. Global and Planetary Change 113, 44–58. https://doi.org/10.1016/j.gloplacha.2013.12.007.

Hay, W.W., 1999. Carbonate sedimentation through the late Precambrian and Phanerozoic. Zentralblatt für Geologie und Paläontologie 435–445. Teil I 5–6 (1998, Heft).

Hay, W.W., Sibuet, J.C., Barron, E.J., et al., 1984. Initial reports of the deep sea drilling project, vol. 75. US Government Printing Office, Washington DC, p. 1303.

Hu, X., Jansa, L., Wang, C., Sarti, M., Bak, K., Wagreich, M., Michalik, J., Soták, J., 2005. Upper Cretaceous oceanic red beds (CORBs) in the Tethys: occurrences, lithofacies, age, and environments. Cretaceous Research 26, 3–20.

Hu, X., Jansa, L., Sarti, M., 2006. Mid-Cretaceous oceanic red beds in the Umbria–Marche Basin, central Italy: Constraints on paleoceanography and paleoclimate. Palaeogeography, Palaeoclimatology, Palaeoecology 233 (3–4), 163–186. https://doi.org/10.1016/j.palaeo.2005.10.003.

Hu, X., Cheng, W., Ji, J., 2009. Origin of Cretaceous Oceanic Red Beds from the Vispi Quarry Section, Central Italy: Visible Reflectance and Inorganic Geochemistry. In: Hu, X., Wang, C., Scott, R.W., Wagreich, M., Jansa, L. (Eds.), Cretaceous Oceanic Red Beds: Stratigraphy, Composition, Origins, Paleoceanographic, and Paleoclimatic Significance, vol. 91. SEPM Spec. Publ., pp. 183–197

Hu, X., Scott, R.W., Cai, Y., Wang, C., M. Dobrinescu, M.C., 2012. Cretaceous oceanic red beds (CORBs): Different time scales and models of origin. Earth-Science Reviews 115 (4), 217–248. https://doi.org/10.1016/j.earscirev.2012.09.007.

Huber, B.T., Petrizzo, M.R., Young, J., Falzoni, F., Galiardoni, S., Bown, P.R., Wade, B.S., 2016. A new online taxonomic database for planktonic foraminifera. Micropaleontology 62, 429–438.

Jarvis, I., 2003. Sample preparation in ICP-MS. In: Jarvis, K.E., Gray, A.L., Houk, R.S. (Eds.), Handbook of Inductively Coupled Plasma Mass Spectrometry, pp. 172–224.

Jarvis, I., Murphy, A.M., Gale, A.S., 2001. Geochemistry of pelagic and hemipelagic carbonates: criteria for identifying systems tracts and sea-level change. Journal of the Geological Society, London 158, 685–696. https://doi.org/10.1144/jgs.158.4.685.

Jarvis, I., Mabrouk, A., Moody, R.T.J., De Cabrera, S.C., 2002. Late Cretaceous (Campanian) carbon isotope events, sea-level change and correlation of the Tethyan and Boreal realms. Palaeogeography, Palaeoclimatology, Palaeoecology 188, 215–248. https://doi.org/10.1016/S0031-0182(02)00578-3.

Jarvis, I., Gale, A.S., Jenkyns, H.C., Pearce, M.A., 2006. Secular variation in Late Cretaceous carbon isotopes: a new δ13C carbonate reference curve for the Cenomanian–Campanian (99.6–70.6 Ma). Geological Magazine 143 (5), 561–608. https://doi.org/10.1017/S0016756806002421.

Jarvis, I., Mabrouk, A., Moody, R.T.J., Murphy, A.M., Sandman, R.I., 2008. Applications of carbon isotope and elemental (Sr/Ca, Mn) chemostratigraphy to sequence analysis: sea-level change and the global correlation of pelagic carbonates. In: Salem, M.J., El-Hawat, A.S. (Eds.), The Geology of East Libya, ume 1. Earth Science Society of Libya, pp. 369–396. Tripoli.

Jarvis, I., Pearce, M.A., Monkenbusch, J., Jurkowska, A., Ullmann, C.V., Dubicka, Z., Thibault, N., 2023. Carbon isotopes, palynology and stratigraphy of the Santonian–Campanian boundary: The GSSP auxiliary sections, Seaford Head (England) and Bocieniec (Poland), and correlation between the Boreal and Tethyan realms. Cretaceous Research 143, 105415. https://doi.org/10.1016/j.cretres.2022.105415.

Jarvis, I., Atar, E., Gröcke, D., Herringshaw, L., Trabucho-Alexandre, J.P., 2024. A global reference for black shale geochemistry and the T-OAE revisited: Upper Pliensbachian – middle Toarcian (Lower Jurassic) chemostratigraphy in the Cleveland Basin, England. Geological Magazine 161, e13. https://doi.org/10.1017/S0016756824000244.

LaGrange, M.T., Konhauser, K.O., Catuneanu, O., Harris, B.S., Playter, T.L., Gingras, M. K., 2020. Sequence stratigraphy in organic-rich marine mudstone successions using chemostratigraphic datasets. Earth-Science Reviews 203, 103137. https://doi.org/10.1016/j.earscirev.2020.103137.

Li, L., Keller, G., Adatte, T., Stinnesbeck, W., 2000. Late Cretaceous sea level changes in Tunisia: a multidisciplinary approach. Journal of the Geological Society of London 157, 447–458. https://doi.org/10.1144/jgs.157.2.447.
Li, Y., Li, C., Guo, J., 2020. Re-evaluation and optimisation of dissolution methods for strontium isotope stratigraphy based on chemical leaching of carbonate certificated reference materials. Microchemical Journal 154, 104607.
Lirer, F., 2000. A new technique for retrieving calcareous microfossils from lithified lime deposits. Micropaleontology 46, 365–369.
Mansour, A., Wagreich, M., 2022. Earth system changes during the cooling greenhouse phase of the Late Cretaceous: Coniacian-Santonian OAE3 sub-events and fundamental variations in organic carbon deposition. Earth-Science Reviews 229, 104022. https://doi.org/10.1016/j.earscirev.2022.104022.
Mansour, A., Gentzis, T., Wagreich, M., Tahoun, S.S., Elewa, A.M.T., 2020. Short-Term Sea Level Changes of the Upper Cretaceous Carbonates: Calibration between Palynomorphs Composition, Inorganic Geochemistry, and Stable Isotopes. Minerals 10 (12), 1099. https://doi.org/10.3390/min10121099.
Martinez-Ruiz, F., Kastner, M., Gallego-Torres, D., Rodrigo-Gámiz, M., Nieto-Moreno, V., Ortega-Huertas, M., 2015. Paleoclimate and paleoceanography over the past 20,000 yr in the Mediterranean Sea Basins as indicated by sediment elemental proxies. Quaternary Science Reviews 107, 25–46. https://doi.org/10.1016/j.quascirev.2014.09.018.
McArthur, J.M., Howarth, R.J., 2024. Strontium isotope stratigraphy of the Cretaceous. In: Hart, M.B., Batenburg, S.J., Huber, B.T., Price, G.D., Thibault, N., Wagreich, M., Walaszczyk, I. (Eds.), Cretaceous Project 200 Volume 1: The Cretaceous World. Geological Society, London, p. 544. https://doi.org/10.1144/sp544-2023-85. Spec. Publ.
McArthur, J.M., Howarth, R.J., Bailey, T.R., 2001. Strontium isotope stratigraphy: LOWESS Version 3: best fit to the marine Sr- isotope curve for 0-509 Ma and accompanying look-up table for deriving numerical age. The Journal of Geology 109, 155–170.
McArthur, J.M., Howarth, R.J., Shields, G.A., 2012. Chapter 7, Strontium Isotope Stratigraphy. In: Gradstein, F.M., Ogg, J.M., Schmitz, M.D., Ogg, G.M. (Eds.), The Geologic Time Scale, 2012. Elsevier, Amsterdam, p. 1144.
Miller, K.G., Wright, J.D., Browning, J.V., 2005. Visions of ice sheets in a greenhouse world. Marine Geology 217, 215–231.
Miniati, F., Petrizzo, M.R., Falzoni, F., Erba, E., 2020. Calcareous plankton biostratigraphy boundary interval in the Bottaccione section (Umbria–Marche Basin, central Italy). Rivista Italiana di Paleontologia e Stratigrafia 126, 771–789.
Mirković, M., Živaljević, M., Đokić, V., Perović, Z., Kalezić, M., Pajović, M., 1985. Geološka karta Crne Gore, 1: 200.000. RSIZ za geološka istraživanja, Titograd.
Nedela-Devide, D., 1957. Značenje globotruncanida za rješevanje nekih stratigrafskih problema u Jugoslaviji. II. kongres geologa Jugoslavije, Sarajevo.
Neuhuber, S., Wagreich, M., 2011. Geochemistry of Cretaceous Oceanic Red Beds — A synthesis. Sedimentary Geology 235 (1–2), 72–78. https://doi.org/10.1016/j.sedgeo.2010.10.008.
Neumann, P., Zacher, W., 2004. The Cretaceous sedimentary history of the Pindos basin (Greece). International Journal of Earth Sciences 93, 119–131. https://doi.org/10.1007/s00531-003-0358-3.
Petrizzo, M.R., 2002. Palaeoceanographic and palaeoclimatic inferences from Late Cretaceous planktonic foraminiferal assemblages from the Exmouth Plateau (ODP Sites 762 and 763, eastern Indian Ocean). Marine Micropaleontology 45, 117–150.
Petrizzo, M.R., 2003. Late Cretaceous planktonic foraminiferal bioevents in the Tethys and in the Southern Ocean record: an overview. Journal of Foraminiferal Research 33 (4), 330–337. https://doi.org/10.2113/0330330.
Petrizzo, M.R., Falzoni, F., Premoli Silva, I., 2011. Identification of the base of the lower–to–middle Campanian Globotruncana ventricosa zone: Comments on reliability and global correlations. Cretaceous Research 32, 387–405. https://doi.org/10.1016/j.cretres.2011.01.010.
Petrizzo, M.R., Wade, B., Gradstein, F.M., 2020. Planktonic foraminifera. In: Gradstein, F.M., Ogg, J.G., Schmitz, M.D., Ogg, G.M. (Eds.), Geologic Time Scale 2020. Elsevier, pp. 74–87.
Petrizzo, M.R., MacLeod, K.G., Watkins, D.K., Wolfgring, E., Huber, B.T., 2022. Late Cretaceous paleoceanographic evolution and the onset of cooling in the Santonian at southern high latitudes (IODP Site U1513, SE Indian Ocean). Paleoceanography and Paleoclimatology 37, e2021PA004353. https://doi.org/10.1029/2021PA004353.
Petrizzo, M.R., King, D.J., Pearson, P.N., Huber, B.T., Wade, B.S., 2025. Planktonic foraminifera in biostratigraphy and biochronology. Newsletters in Stratigraphy. https://doi.org/10.1127/nos/2024/0840 published online Oct 17, 2024.
Premoli Silva, I., Sliter, W.V., 1995. Cretaceous planktonic foraminiferal biostratigraphy and evolutionary trends from the Bottaccione section. Gubbio, Italy. Palaeontographia Italica 82, 1–89.
Premoli Silva, I., Sliter, W.V., 1999. Cretaceous paleoceanography: evidence from planktonic foraminiferal evolution. In: Barrera, E., Johnson, C.C. (Eds.), Evolution of the Cretaceous Ocean-Climate System, vol. 332. Geological Society of America, Special Paper, Colorado, Boulder., pp. 301–328
Premoli Silva, I., Verga, D., 2004. Practical Manual of Cretaceous Planktonic Foraminifera. In: Verga, D., Rettori, R. (Eds.), International School on Planktonic Foraminifera, Universities of Perugia & Milano. Tipografia Pontefelcino, Perugia, p. 283.
Renard, M., Rafélis, M.D., Emmanuel, L., Beltran, C., Moullade, M., Tronchetti, G., 2007. Fluctuations of sea-water chemistry during Gargasian (Middle Aptian) time. Data from trace element content (Mg, Sr, Mn, Fe) in hemipelagic carbonates from La Marcouline Quarry (Cassis, SE France). Carnets de Géologie 2007 (3), 1–28.
Robaszynski, F., Caron, M., 1995. Foraminiferes planctoniques du Crétacé: commentaire de la zonation Europe-Méditerranée. Bulletin de la Societe Geologique de France 166, 681–692.
Sabatino, N., Meyers, S.R., Voigt, S., Coccioni, R., Sprovieri, M., 2018. A new high–resolution carbon–isotope stratigraphy for the Campanian (Bottaccione section): Its implications for global correlation, ocean circulation, and astrochronology. Palaeogeography, Palaeoclimatology, Palaeoecology 489, 29–39. https://doi.org/10.1016/j.palaeo.2017.08.026.
Sames, B., Wagreich, M., Conrad, C.P., Iqbal, S., 2020. Aquifer-eustasy as the main driver of short-term sea-level fluctuations during Cretaceous hothouse climate phases. Geological Society, London, Special Publications 498 (1), 9–38. https://doi.org/10.1144/SP498-2019-105.
Schmid, S.M., Bernoulli, D., Fügenschuh, B., Matenco, L., Schefer, S., Schuster, R., Tischler, M., Ustaszewski, K., 2008. The Alpine-Carpathian-Dinaridic orogenic system: correlation and evolution of tectonic units. Swiss Journal of Geosciences 101, 139–183. https://doi.org/10.1007/s00015-008-1247-3.
Schmid, S.M., Fügenschuh, B., Kounov, A., Maţenco, L., Nievergelt, P., Oberhänsli, R., Pleuger, J., Schefer, S., Schuster, R., Tomljenović, B., Ustaszewski, K., van Hinsbergen, D.J.J., 2020. Tectonic units of the Alpine collision zone between Eastern Alps and western Turkey. Gondwana Research 78, 308–374. https://doi.org/10.1016/j.gr.2019.07.005.
Schoepfer, S.D., Shen, J., Wei, H., Tyson, R.V., Ingall, E., Algeo, T.J., 2015. Total organic carbon, organic phosphorus, and biogenic barium fluxes as proxies for paleomarine productivity. Earth-Science Reviews 149, 23–52.
Schöllhorn, I., Adatte, T., Van de Schootbrugge, B., Houben, A., Charbonnier, G., Janssen, N., Föllmi, K.B., 2020. Climate and environmental response to the break-up of Pangea during the Early Jurassic (Hettangian-Pliensbachian); the Dorset coast (UK) revisited. Global and Planetary Change 185. https://doi.org/10.1016/j.gloplacha.2019.103096.
Scott, R.W., Hu, X., Bubik, M., Malata, E., Melinte, M., Sanders, D., Shcherbinina, E., Skupien, P., Wagreich, M., 2005. Depositional timing and rates of Cretaceous oceanic red beds. In: 7th International Symposium on the Cretaceous, Neuchatel, Switzerland, September 5–9, Scientific Program and Abstracts, pp. 199–200.
Soua, M., 2010. Productivity and bottom water redox conditions at the Cenomanian-Turonian Oceanic Anoxic Event in the southern Tethyan margin, Tunisia. Revue méditerranéenne de l'environnement 4, 653–664.
Sprovieri, M., Sabatino, N., Pelosi, N., Batenburg, S.J., Coccioni, R., Iavarone, M., Mazzola, S., 2013. Late Cretaceous orbitally–paced carbon isotope stratigraphy from the Bottaccione Gorge (Italy). Palaeogeography, Palaeoclimatology, Palaeoecology 379–380, 81–94. https://doi.org/10.1016/j.palaeo.2013.04.006.
Stampfli, G.M., Borel, G.D., 2002. A plate tectonic model for the Paleozoic and Mesozoic constrained by dynamic plate boundaries and restored synthetic oceanic isochrons. Earth and Planetary Science Letters 196 (1–2), 17–33.
Stampfli, G.M., Borel, G.D., 2004. The TRANSMED transects in space and time: constraints on the paleotectonic evolution of the Mediterranean domain. In: Cavazza, W., Roure, F., Spakman, W., Stampfli, G.M., Ziegler, P. (Eds.), The TRANSMED Atlas: The Mediterranean Region from Crust to Mantle. Springer, pp. 53–80.
Taylor, S.R., McLennan, S.M., 2001. Chemical composition and element distribution in the Earth's crust. In: Meyers, R.A. (Ed.), Encyclopedia of Physical Science and Technology, third ed. Academic Press, San Diego, pp. 697–719.
Thibault, N., Jarvis, I., Voigt, S., Gale, A.S., Attree, K., Jenkyns, H.C., 2016. Astronomical calibration and global correlation of the Santonian (Cretaceous) based on the marine carbon isotope record. Paleoceanography 31, 847–865. https://doi.org/10.1002/2016PA002941.
van Hinsbergen, D.J.J., de Groot, L.V., van Schaik, S.J., Spakman, W., Bijl, P.K., et al., 2015. A Paleolatitude Calculator for Paleoclimate Studies. PLoS One 10 (6), e0126946. https://doi.org/10.1371/journal.pone.0126946.
Wagreich, M., 2009. Coniacian-Santonian oceanic red beds and their link to Oceanic Anoxic Event 3. In: Hu, X., Wang, C., Scott, R.W., Wagreich, M., Jansa, L. (Eds.), Cretaceous Oceanic Red Beds: Stratigraphy, Composition, Origins, and Paleoceanographic and Paleoclimatic Significance, vol. 91. SEPM Spec. Publ., pp. 235–242
Wagreich, M., Koukal, V., 2020. The pelagic archive of short-term sea-level change in the Cretaceous: a review of proxies linked to orbital forcing. In: Wagreich, M., Hart, M., Sames, B., Yilmaz, I.O. (Eds.), Cretaceous Climate Events and Short-Term Sea-Level Changes. Geological Society. Spec. Publ, London, p. 498. https://doi.org/10.1144/SP498-2019-34.
Wagreich, M., Krenmayr, H.G., 2005. Upper Cretaceous oceanic red beds (CORB) in the Northern Calcareous Alps (Nierental Formation, Austria): slope topography and clastic input as primary controlling factors. Cretaceous Research 26, 57–64. https://doi.org/10.1016/j.cretres.2004.11.012.
Wang, C., Hu, X., Huang, Y., Scott, R., Wagreich, M., 2009. Cretaceous Oceanic Red Beds (CORB): A Window on Global Oceanic/Climatic Change. In: Hu, X., Wang, C., Scott, R.W., Wagreich, M., Jansa, L. (Eds.), Cretaceous Oceanic Red Beds: Stratigraphy, Composition, Origins and Paleoceanographic and Paleoclimatic Significance, vol. 91. SEPM Spec. Pub., pp. 13–33
Wang, C., Hu, X., Huang, Y., Wagreich, M., Scott, R.W., Hay, W.W., 2011. Cretaceous oceanic red beds as possible consequence of oceanic anoxic events. Sedimentary Geology 235 (1–2), 27–37.
Wendler, I., 2013. A critical evaluation of carbon isotope stratigraphy and biostratigraphic implications for Late Cretaceous global correlation.

Earth-Science Reviews 126, 116–146. https://doi.org/10.1016/j.earscirev.2013.08.003.
Wendler, J.E., Wendler, I., Vogt, C., Kuss, J., 2016. Link between cyclic eustatic sea-level change and continental weathering: evidence for aquifer-eustasy in the Cretaceous. Palaeogeography, Palaeoclimatology, Palaeoecology 441, 430–437. https://doi.org/10.1016/j.palaeo.2015.08.014.
Wolfgring, E., Wagreich, M., Dinarès-Turell, J., Yilmaz, I.O., Böhm, K., 2017. Plankton biostratigraphy and magnetostratigraphy of the Santonian–Campanian boundary interval in the Mudurnu-Göynük Basin, northwestern Turkey. Cretaceous Research 87, 296–311. https://doi.org/10.1016/j.cretres.2017.07.006.
Wolfgring, E., Wagreich, M., Dinarès Turell, J., Gier, S., Böhm, K., Sames, B., Spötl, C., Popp, F., 2018. The Santonian–Campanian boundary and the end of the Long Cretaceous Normal Polarity–Chron: isotope and plankton stratigraphy of a pelagic reference section in the NW Tethys (Austria). Newsletters on Stratigraphy 51, 445–476. https://doi.org/10.1127/nos/2018/0392.
Wolfgring, E., Wagreich, M., Hohenegger, J., Böhm, K., Dinarès Turell, J., Gier, S., Sames, B., Spötl, C., Jin, S., 2021. An integrated multi-proxy study of cyclic pelagic deposits from the north-western Tethys: The Campanian of the Postalm section (Gosau Group, Austria). Cretaceous Research 120, 104704. https://doi.org/10.1016/j.cretres.2020.104704.

Appendix A. Supplementary data

Supplementary data to this article can be found online at https://doi.org/10.1016/j.cretres.2025.106194.

Appendix 1

Cross plots of the correlation coefficients for the selected major and trace elements, carbon and oxygen isotopes. Data are distributed within separate lithostratigraphic units to better illustrate geochemical variation.

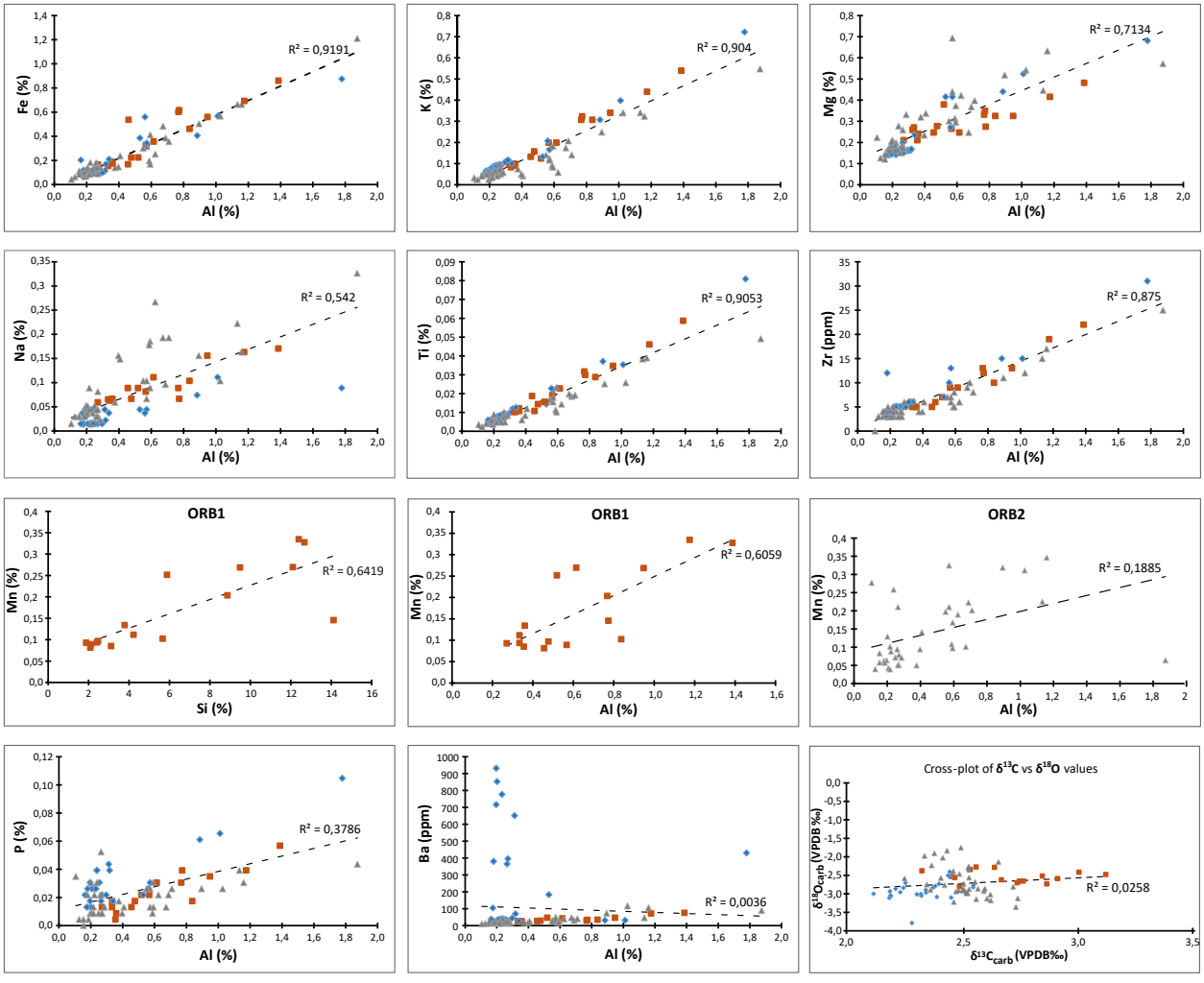

Appendix 2

Si/Al diagram showing the possible origin of silica in the Čanj section (after Barbera et al., 2006).

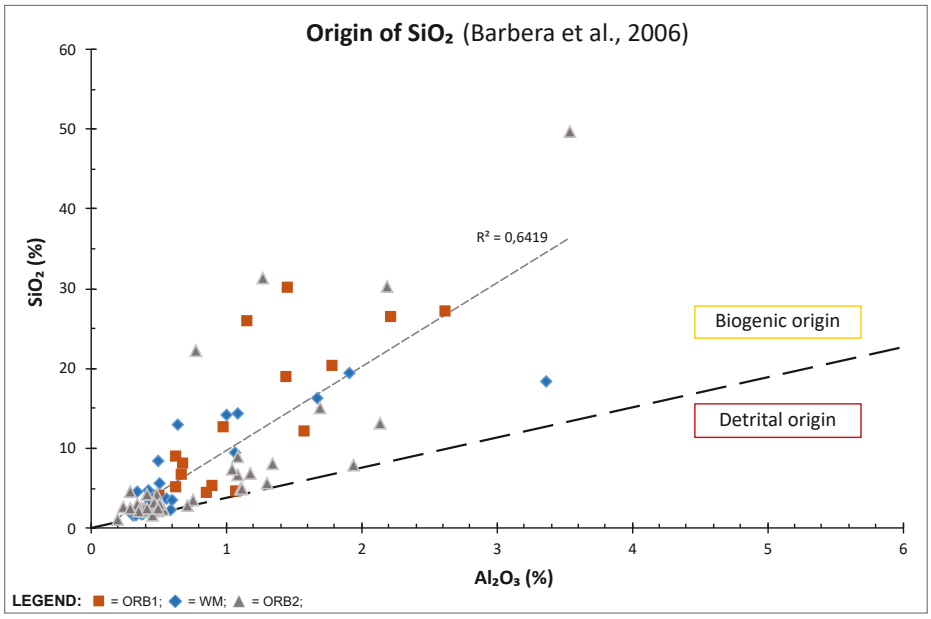

Appendix 3

Archaeoglobigerina Pessagno 1967
Archaeoglobigerina cretacea (d'Orbigny, 1840)
Contusotruncana fornicata (Plummer, 1931)
Contusotruncana morozovae (Vasilenko, 1961)
Contusotruncana patelliformis (Gandolfi, 1955)
Contusotruncana plummerae (Gandolfi, 1955)
Dicarinella Porthault, in Donze et al. (1970
Dicarinella asymetrica (Sigal, 1952)
Dicarinella concavata (Brotzen, 1934)
Globotruncana Cushman 1927
Globotruncana arca (Cushman, 1926)
Globotruncana bulloides Vogler, 1941
Globotruncana linneiana (d'Orbigny, 1839)
Globotruncana neotricarinata Petrizzo, Falzoni & Premoli Silva, 2011
Globotruncana ventricosa (White, 1928)
Globotruncanita atlantica (Caron, 1972)
Globotruncanita conica (White, 1928)
Globotruncanita elevata (Brotzen, 1934)
Globotruncanita stuartiformis (Dalbiez, 1955)
Laeviella bolli (Pessagno, 1967)
Laeviheterohelix Nederbragt 1991
Marginotruncana Hofker 1956
Marginotruncana cf. *angusticarenata* (Gandolfi, 1942)
Marginotruncana cf. *undulata* (Lehmann, 1963)
Marginotruncana coronata (Bolli, 1945)
Marginotruncana pseudolinneiana Pessagno, 1967
Marginotruncana pseudomarginata Neagu 2012
Marginotruncana renzi (Gandolfi, 1942)
Marginotruncana sigali (Reichel, 1950)
Marginotruncana sinuosa Porthault, in Donze et al. (1970
Marginotruncana tarfayaensis (Lehmann, 1963)
Muricohedbergella Huber and Leckie 2011
Muricohedbergella flandrini (Porthault, in Donze et al., 1970)
Planohedbergella prairiehillensis (Pessagno, 1967)
Planohedbergella ultramicra (Subbotina, 1949)
Planoheterohelix Georgescu and Huber 2009
Planoheterohelix globulosa (Ehrenberg, 1840)
Pseudoguembelina Bronniman and Brown 1953
Pseudotextularia Rzehak 1891
Ventilabrella Cushman 1928